Contrasting effects of intralocus sexual conflict on sexually antagonistic coevolution

Pennell, Tanya M; de Haas, Freek J H; Morrow, Edward H; van Doorn, Gerrit

Published in:
Proceedings of the National Academy of Sciences of the United States of America

DOI:
10.1073/pnas.1514328113

Contrasting effects of intralocus sexual conflict on sexually antagonistic coevolution

Tanya M. Pennell[a], Freek J. H. de Haas[b], Edward H. Morrow[a], and G. Sander van Doorn[b,1]

[a]School of Life Sciences, University of Sussex, Brighton BN1 9RH, United Kingdom; and [b]Groningen Institute for Evolutionary Life Sciences, University of Groningen, 9700 CC Groningen, The Netherlands

Edited by Brian Charlesworth, University of Edinburgh, Edinburgh, United Kingdom, and approved December 17, 2015 (received for review July 21, 2015)

Evolutionary conflict between the sexes can induce arms races in which males evolve traits that are detrimental to the fitness of their female partners, and vice versa. This interlocus sexual conflict (IRSC) has been proposed as a cause of perpetual intersexual antagonistic coevolution with wide-ranging evolutionary consequences. However, theory suggests that the scope for perpetual coevolution is limited, if traits involved in IRSC are subject to pleiotropic constraints. Here, we consider a biologically plausible form of pleiotropy that has hitherto been ignored in treatments of IRSC and arrive at drastically different conclusions. Our analysis is based on a quantitative genetic model of sexual conflict, in which genes controlling IRSC traits have side effects in the other sex, due to incompletely sex-limited gene expression. As a result, the genes are exposed to intralocus sexual conflict (IASC), a tug-of-war between opposing male- and female-specific selection pressures. We find that the interaction between the two forms of sexual conflict has contrasting effects on antagonistic coevolution: Pleiotropic constraints stabilize the dynamics of arms races if the mating traits are close to evolutionary equilibrium but can prevent populations from ever reaching such a state. Instead, the sexes are drawn into a continuous cycle of arms races, causing the buildup of IASC, alternated by phases of IASC resolution that trigger the next arms race. These results encourage an integrative perspective on the biology of sexual conflict and generally caution against relying exclusively on equilibrium stability analysis.

sexual conflict | arms race | intersexual additive genetic correlation | sex-differential expression | pleiotropy

The sexes have followed distinct evolutionary trajectories due to divergent selection regimes that have led to, and been exaggerated by, anisogamy (1–4). This disparity has the potential to ignite two forms of sexual conflict (5): interlocus and intralocus sexual conflict (IRSC and IASC, respectively). Both forms of conflict have been described as independent drivers of divergence and speciation (5–8) and have important implications for the rate of trait evolution, the maintenance of genetic variation, and sexual selection (9–12).

IRSC arises from a direct interaction between the sexes that increases the fitness of one sex at the expense of the other. Typically, males evolve adaptations for success in sperm competition and monopolization of females (male offense traits), which often prevents females from obtaining fitness benefits through polyandry or sperm use (13–15). Subsequently, an arms race is initiated via the evolution of female counteradaptations that reduce the fitness loss (female defense traits) (14, 16). Repeated or even perpetual cycles of counteradaptation in each sex are predicted to follow over evolutionary time, leading to the rapid evolution of reproductive traits (6, 7).

Whereas IRSC clearly manifests itself as a form of conflict in mating interactions, IASC involves a more subtle type of sexual antagonism that operates at the level of phenotype expression. Here, conflict arises because the sexes share the same genome but are nevertheless under selection to express different, sex-specific phenotypes (4, 17, 18). The resolution of IASC can be achieved via the evolution of sexual dimorphism (2, 19–21). However, the observation of negative intersexual correlations for fitness indicates that appreciable levels of IASC are maintained (22–25), both in the wild (11, 26, 27) and in laboratory populations (28–31).

Given their different modes of operation, IASC and IRSC are traditionally considered as separate forces. In fact, in typical studies of IASC, fitness is frequency-independent and determined by a univariate trait, ruling out the possibility of coevolution between offense and defense traits characteristic of IRSC. Models of IRSC, however, consider interactions between at least two phenotypic characters expressed in a mating context, where the strategy of one sex is governed by a different set of loci from the trait(s) required by the other sex to counteradapt (6). This has commonly been interpreted to imply that loci involved in IRSC have sex-limited expression (5, 7, 10, 32, 33) and are, therefore, unaffected by IASC. Nevertheless, some authors have emphasized the role of pleiotropic side effects, which may not be restricted to a single sex, in stabilizing the dynamics of intersexual antagonistic coevolution (8, 32).

For instance, if the evolution of female indifference to a male mating signal is mediated by mutations in the female's sensory system (9, 10), then those same mutations might be expressed in males as well. If so, potential negative side effects (such as a reduced foraging efficiency) of female counteradaptations to sexual conflict are subject to selection in both sexes. As in this example, many traits involved in sexual conflict have a complex genetic basis, providing ample opportunity for pleiotropic effects between male and female traits, by which the two processes of conflict can become linked. The potential that the same loci underlie

Significance

Biologists distinguish two forms of conflict between the sexes, recognized as separate drivers of rapid evolution and diversification. Sexual conflict manifests itself as a tug-of-war between selective forces acting on genes jointly expressed by males and females, allowing neither to maximize their fitness. It also appears in mating interactions, where males and females engage in evolutionary arms races to increase their reproductive success to the detriment of their partner. We model the plausible scenario that reproductive traits are involved in both types of conflict and show that their interaction can draw the sexes into perpetual cycles of escalation, alternated by phases of conflict resolution. This result sheds light on the maintenance of sexually antagonistic variation and the complex dynamics of male–female coevolution.

Author contributions: T.M.P., E.H.M., and G.S.v.D. designed research; T.M.P., F.J.H.d.H., and G.S.v.D. performed research; F.J.H.d.H. and G.S.v.D. analyzed data; and T.M.P., F.J.H.d.H., E.H.M., and G.S.v.D. wrote the paper.

The authors declare no conflict of interest.

This article is a PNAS Direct Submission.

[1]To whom correspondence should be addressed. Email: g.s.van.doorn@rug.nl.

This article contains supporting information online at www.pnas.org/lookup/suppl/doi:10.1073/pnas.1514328113/-/DCSupplemental.

both forms of conflict is further increased by the widespread occurrence of alleles associated with IASC or IRSC throughout the genome (30, 34–36). Moreover, both IASC and IRSC are predicted to stem predominantly from reproductive traits, where the evolutionary interests of the sexes diverge the most (22), although sexually dimorphic traits may, in fact, be subject to reduced IASC due to the prior evolution of sex-specific gene regulation (12, 20).

The potential for IRSC and IASC to interact has been highlighted recently (4), where it was noted that intersexual selection acting on a trait that is genetically correlated between the sexes would often give rise to intralocus sexual conflict. It was also argued that the outcome of this interaction would depend on the opportunity for IASC resolution: IASC could persist and therefore prevent counteradaptation of the trait in response to IRSC, or IASC could be resolved, resulting in the escalation of arms races stemming from IRSC. We here develop a formal, quantitative genetic model of traits involved in inter- and intralocus sexual conflict, to verify these arguments and examine their implications for the evolution of sexual conflict. Our analysis supports the intuition that IASC can stabilize antagonistic male–female coevolution but also indicates that the consequences of interaction between the two forms of sexual conflict reach much further than anticipated. Finally, we discuss the implications of these results for the occurrence of perpetual arms races and the maintenance of sexually antagonistic variation in fitness.

The Model

Biological Assumptions. Our analysis builds on a model of sexually antagonistic coevolution introduced by Rowe et al. in 2005 (32) (henceforth referred to as RCD05). The biological scenario considered in their study is that males and females are in conflict over the rate of mating, which is taken to be an increasing sigmoid function $\psi(s) = 1/(1+\exp(-s))$ of the intensity of a mating stimulus, s. This particular formulation of the model captures the situation that mating is a contest between male offense and female defense traits, in which more extreme offense traits increase the rate of mating, whereas more extreme defense traits have the opposite effect. Biological examples of offense and defense traits include grasping and antigrasping devices, as seen in water striders (13), or traumatic insemination and counteradaptations to control its harmful effects, as found in bedbugs (16) and (hermaphroditic) land snails (14).

In RCD05, the intensity of the mating stimulus perceived by a female is taken to be a function of three evolving phenotypic traits with sex-limited expression. Specifically, $s = z_{♀} \times (y_{♂} - x_{♀})$ depends on the difference between a persistence trait, $y_{♂}$, expressed in males, and a female resistance trait, $x_{♀}$, reflecting the threshold amount of persistence required to induce mating. In addition, the perceived intensity of the mating stimulus depends on the sensitivity of the female, $z_{♀}$, which quantifies how strongly she discriminates between males that differ in their level of persistence. Male sexual fitness is modeled as an increasing function of the mating rate, such that sexual selection will invariably favor males who mate at a higher frequency. In contrast, females are assumed to achieve maximal reproductive success at an intermediate mating rate θ_{ψ}. Selection may therefore act on females to reduce their rate of mating by increasing the mating threshold or evolving insensitivity to the mating stimulus. The latter response is likely when there are no pleiotropic constraints that prevent females from adjusting their sensitivity (32). However, the sensory system underlying female mating behavior is probably important in other contexts as well, such that the maximization of female reproductive success may have negative consequences for fitness components unrelated to mating interactions. Similarly, evolving higher levels of persistence is presumably associated with increasing costs for males. To capture these effects, each of the mating traits is assumed to be subject to stabilizing natural selection for an intermediate optimum.

In this paper, the analysis of RCD05 is extended in two ways. First, if the mating characters have pleiotropic effects, then these need not necessarily be restricted to one sex. Therefore, we take into account that female resistance and sensitivity genes are expressed in males, denoting the corresponding phenotypic trait values as $x_{♂}$ and $z_{♂}$, respectively. Likewise, male persistence genes affect a correlated phenotypic character in females, for which the trait value is denoted as $y_{♀}$. Stabilizing natural selection acts on x, y, and z in both sexes in our model. The optimum trait values and the strength of stabilizing selection are allowed to differ between males and females. Note that x, y, and z still have sex-limited effects on the mating rate (as in RCD05), because their expression in the context of intersexual interactions is contingent on the asymmetry between male and female sex roles.

As a second extension, our model also considers the dynamics of arms races in cases where mating requires complementarity or matching of male and female mating characters. This alternative mating mechanism, which has frequently been considered in models of sexual conflict (8), is modeled by defining the mating rate as a unimodal function $\psi(s) = \exp(-s^2/2)$ of the mating stimulus $s = z_{♀} \times (y_{♂} - x_{♀})$ (which here reflects the extent to which the male differs from the female's preferred phenotype). As in sexual selection models, $x_{♀}$ can then be interpreted as a female mating preference, $y_{♂}$ as a male mating trait (e.g., an ornament) on which the preference acts, and $z_{♀}$ as a measure of female choosiness. For simplicity, we will continue to refer to the mating characters as threshold, persistence, and sensitivity, as in RCD05, except when we are explicitly considering complementarity-based mating (in which case we will use preference, ornament, and choosiness instead). Examples of sexually antagonistic mating systems that could be considered as complementarity-based include penis length/female reproductive tract coevolution in waterfowl (3), and male seminal protein/female receptor coevolution in fruit flies (37).

A key feature of our model is that genes involved in IRSC are subject to distinct components of selection in males and females. As a result, selection is likely to favor different optimum trait values in the two sexes, setting the stage for IASC to occur. Prolonged IASC is expected when only a small fraction of the genes are regulated in a sex-specific manner, making it more difficult for males and females to diverge toward their sex-specific optima (2, 19, 23). The strength of the phenotypic correlation between brothers and sisters in their expression of a mating trait and the corresponding correlated character provides an observable measure of the degree of sex-differential expression. Additive genetic intersexual correlation coefficients, which can be inferred from comparisons between opposite-sex relatives (11, 18), therefore play a prominent role as control parameters in our further analysis: Their effect on the rate of IASC resolution allows us to systematically vary the impact of IASC on antagonistic male–female coevolution.

Mathematical Representation. Based on fitness functions that capture the above biological assumptions, we calculated the strength of selection acting on each of the characters and used this information to determine their rate of evolution (*Materials and Methods*). The evolutionary dynamics of the population average trait values is described by a multivariate breeder's equation (38), $d\mathbf{u}/dt = \mathbf{G}\,\boldsymbol{\beta}(\mathbf{u})$, where $\mathbf{u}$ is a (column) vector $(\bar{x}_{♀}, \bar{z}_{♀}, \bar{y}_{♂}, \bar{x}_{♂}, \bar{z}_{♂}, \bar{y}_{♀})^{\mathrm{T}}$ containing the average trait values and $\mathbf{G}$ is the additive genetic variance–covariance matrix. This matrix depends on the intersexual correlations r_x, r_y, and r_z, as specified

in Eq. **4** in *Materials and Methods*. The vector $\boldsymbol{\beta}(\mathbf{u})$ is the selection gradient, given by

$$\boldsymbol{\beta}(\mathbf{u}) = \begin{pmatrix} a\,\bar{z}_{♀}\,(\overline{\psi} - \theta_{\psi})\,\overline{\psi}' - c_{x_{♀}}\,(\bar{x}_{♀} - \theta_{x_{♀}}) \\ a\,(\bar{x}_{♀} - \bar{y}_{♂})\,(\overline{\psi} - \theta_{\psi})\,\overline{\psi}' - c_{z_{♀}}\,(\bar{z}_{♀} - \theta_{z_{♀}}) \\ b\,\bar{z}_{♀}\,\overline{\psi}' - c_{y_{♂}}\,(\bar{y}_{♂} - \theta_{y_{♂}}) \\ -c_{x_{♂}}\,(\bar{x}_{♂} - \theta_{x_{♂}}) \\ -c_{z_{♂}}\,(\bar{z}_{♂} - \theta_{z_{♂}}) \\ -c_{y_{♀}}\,(\bar{y}_{♀} - \theta_{y_{♀}}) \end{pmatrix}. \qquad [1]$$

Each element of the vector $\boldsymbol{\beta}(\mathbf{u})$ quantifies the marginal fitness effect of varying one of the characters by one phenotypic unit, in the context of the current population with average trait values $\mathbf{u}$. The upper three elements represent selection gradients acting on the mating traits $\bar{x}_{♀}$, $\bar{z}_{♀}$, and $\bar{y}_{♂}$, which depend on the fitness effects of mating interactions. The strength of sexual selection varies with $\overline{\psi}$ and $\overline{\psi}'$, the values of the mating rate function and its first derivative at $\bar{s} = \bar{z}_{♀} \times (\bar{y}_{♂} - \bar{x}_{♀})$. In addition, the impact of mating on female and male fitness is scaled by two parameters, a and b, that quantify, respectively, the cost to females of deviating from their optimum mating rate and the strength of the association between mating rate and male reproductive success. Direct selection on the correlated characters, reflected by the lower three elements of the selection gradient, occurs only in the form of stabilizing natural selection, which also acts on the mating traits. Stabilizing natural selection is parameterized for each trait by an optimum trait value θ and a selection intensity c, which determines how much fitness decreases when a phenotype is displaced by a given amount from its viability selection optimum.

Results

The coevolution of the mating characters $\bar{x}_{♀}$, $\bar{z}_{♀}$, and $\bar{y}_{♂}$ in the absence of between-sex pleiotropy has been analyzed by RCD05, and we briefly recapitulate their results before examining the interaction between IRSC and IASC. A key finding is that IRSC, acting by itself, has multiple potential evolutionary outcomes (8, 32). These include escalating arms races, the evolution of female indifference to the mating stimulus, and continual coevolution of threshold, persistence, and sensitivity. Female indifference tends to evolve when females are able to adjust the shape of their preference function without major negative side effects, enabling them to avoid large fitness costs of IRSC at evolutionary equilibrium. By contrast, evolutionary arms races, which result in a significant reduction of female fitness, occur when adaptation of the female sensory system is constrained by a lack of genetic variation or strong stabilizing selection on sensitivity in contexts other than mating. Hence, RCD05 conclude that the outcome of IRSC depends critically on the constraints and selective forces that act on the female preference function.

Evolutionary Equilibria Are Stabilized by IASC. Following Pennell and Morrow (4), we hypothesized that IASC would restrain IRSC in cases with between-sex pleiotropic trait expression, potentially preventing the escalation of arms races. In particular, if the intersexual correlations are high and strong stabilizing selection acts on the correlated characters $\bar{x}_{♂}$, $\bar{z}_{♂}$, and $\bar{y}_{♀}$, IASC is predicted to keep the mating traits fixed at an evolutionary equilibrium even if this would not be stable under the sole action of IRSC. To see why, suppose that one or several of the mating traits evolve away from the equilibrium under the influence of intersexual selection (i.e., sexual selection generated by variation in ψ). This change is associated with a correlated change of the homologous characters, causing those to deviate from their viability selection optimum. As a result, the response to sexual selection is opposed by stabilizing natural selection in the other sex, which pushes the traits back to their original values if the pleiotropic fitness effects outweigh the selective forces resulting from IRSC.

A formal equilibrium and stability analysis confirms this verbal argument (*SI Appendix*), demonstrating that IASC can stabilize the dynamics of IRSC in the vicinity of evolutionary equilibria that would otherwise be unstable. In such cases, IASC prevents the sexes from being engaged in an escalating arms race and allows them to sustain a stable "truce." The main prerequisite for stabilization is that the intersexual genetic correlations and selection on the correlated characters must be sufficiently strong in the direction in phenotype space along which the arms race would have otherwise unfolded, so that stabilizing natural selection is capable of overpowering the forces generated by IRSC.

The mathematical analysis leads to two additional insights. First, neither the location nor the number of fixed points depends on the values of the intersexual genetic correlations. As a result, the evolutionary equilibria of the mating characters are determined by sexual selection and within-sex stabilizing natural selection, exactly as in RCD05, whereas the equilibrium values of the correlated characters are simply given by their respective optimum trait values $\theta_{x_{♂}}$, $\theta_{z_{♂}}$, and $\theta_{y_{♀}}$. Apart from being useful to characterize the evolutionary equilibria, this insight also restricts the range of phenomena that can be associated with qualitative changes in the dynamics of IRSC due to its interaction with IASC. Specifically, from the mathematical theory of qualitative changes in dynamical systems [bifurcation theory (39)], we infer that variation of the intersexual correlations can induce no other generic local bifurcation than a so-called Poincaré–Andronov–Hopf bifurcation, given that all other options require equilibria to move relative to one another. This bifurcation is associated with the emergence or disappearance of a cycle (i.e., periodic orbit), which can either act as an alternative evolutionary attractor or restrict the attainability of certain evolutionary outcomes. Hence, if IASC induces a qualitative change in the stability of an equilibrium, the associated appearance or loss of a cycle could dramatically alter the outcome of sexual conflict.

Dynamics of Sexual Conflict Away from Equilibria. To complement the insights offered by the local stability analysis, we studied the global evolutionary dynamics of the mating characters based on numerical solutions calculated for the two mating scenario variants of the model. Fig. 1 shows an illustrative result for the case when mating is a contest between offense and defense traits. Here, IRSC leads to continuous fluctuations in the male persistence trait and the female sensitivity and mating threshold (cf. figure 5b in ref. 32). During these evolutionary cycles, the initiation of arms races between threshold and persistence is alternated by the evolution of female indifference to the mating stimulus, inducing the threshold and persistence trait to evolve back toward their optimal trait value under natural selection. The oscillations persist in the presence of low levels of pleiotropic expression between the sexes (Fig. 1*A*), but their amplitude decreases if the intersexual genetic correlations are stronger. In that case, fluctuations of the mating traits induce a larger correlated selection response that is opposed more strongly by stabilizing selection in the other sex. Modest-to-high values of the intersexual correlations [still below typical empirically observed values (20)] entirely prevent the initiation of arms races, causing the trait values to converge on a stable equilibrium (Fig. 1*B*). These results are in line with the conclusions of the mathematical analysis: Without changing the location of the equilibrium, IASC has induced an evolutionary repellor, surrounded by a stable periodic solution, to transform into a stable fixed point that attracts the dynamics in Fig. 1*B*. Moreover, the qualitative change in the stability of the equilibrium is associated with the disappearance of the periodic attractor present in Fig. 1*A*.

More puzzling to explain are the simulation results obtained for the model variant with complementarity-based mating, illustrated in Fig. 2. Here, again, Fig. 2*A* shows the outcome of evolution when the intersexual genetic correlations are weak. In

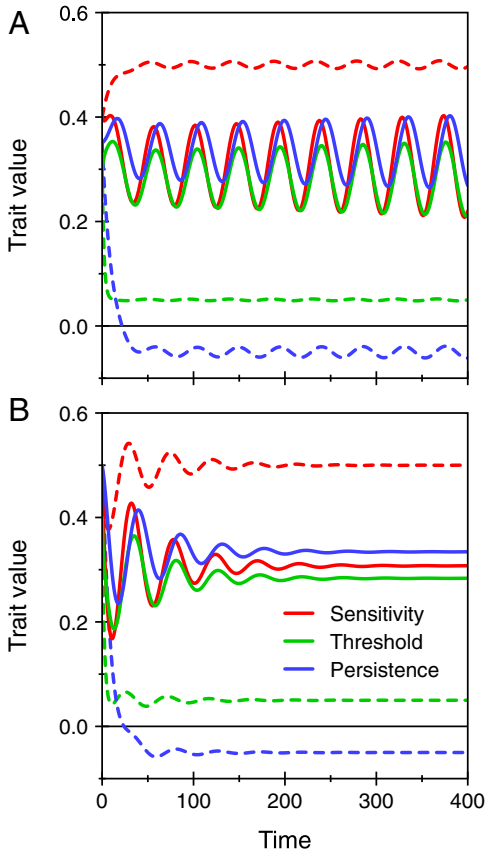

Fig. 1. IASC stabilizes sexually antagonistic coevolution of offense and defense traits. Male and female mating traits (solid lines) covary with their respective homologous character in the other sex (dashed lines) as a result of between-sex pleiotropic gene expression. The population-average trait values converge on an evolutionary cycle when the intersexual genetic correlations are low (*A*) but are driven toward a stable equilibrium (*B*) when sensitivity and threshold are subject to stronger IASC. Parameters are $a=5$, $b=0.5$, $\theta_{x_\varphi}=\theta_{x_\sigma}=0.05$, $\theta_{y_\varphi}=\theta_{y_\sigma}=-0.05$, $\theta_{z_\varphi}=\theta_{z_\sigma}=0.5$, $\theta_\psi=0.2$, $c_{x_\varphi}=c_{x_\sigma}=0.5$, $c_{y_\varphi}=c_{y_\sigma}=c_{z_\varphi}=c_{z_\sigma}=0.1$. In *A*, $r_x=r_z=0.1$ and $r_y=0.2$; in *B*, $r_x=r_z=0.5$ and $r_y=0.2$.

this case, females evolve costly choosiness, and we observe an arms race to exaggerated levels of ornamentation and corresponding costly preferences. Eventually, the sexes converge on a stable equilibrium, at which chase-away sexual selection (9, 10) favoring further exaggeration is balanced by natural selection acting in the opposite direction. Antagonistic coevolution can escalate in two directions and thereby converge on two different fixed points (shown in Fig. 2*A*, *Upper* and *Lower*). When the intersexual correlations are high (Fig. 2*B*), such that female choice is subject to strong pleiotropic constraints, arms races driven by chase-away sexual selection occur as well, but they are more effectively halted by natural selection, as a consequence of stronger pleiotropic side effects in the other sex. However, as the interlocus sexual conflict built up by the arms race is resolved, sexual selection on the female preference and male ornamentation changes direction, suddenly triggering an arms race in the opposite direction. As a result, rather than stabilizing the dynamics of IRSC, IASC prevents the coevolving sexes from reaching evolutionary equilibria, so that males and females are caught in a recurrent evolutionary cycle (thick lines in Fig. 2*B*).

At first sight, these results seem to contradict the conclusions from the mathematical analysis, which stated that stable equilibria of IRSC cannot be destabilized by IASC. However, the arms races observed in Fig. 2*B* never get close to the endpoints of the coevolutionary chase in Fig. 2*A*, so we cannot yet infer the stability properties of the equilibria. We therefore ran simulations from other initial conditions, closer to the endpoints reached by evolution in Fig. 2*A*. The additional simulations (thin lines in Fig. 2*B*, *Upper* and *Lower*) indicate that the sexes can still attain the same stable state characterized by exaggerated trait expression when the intersexual correlations are strong. In other words, no differences exist between Fig. 2*A* and Fig. 2*B* in the stability properties of the evolutionary equilibria, consistent with the analytical results. We are thus led to conclude that IASC has consequences for the dynamics of sexually antagonistic coevolution far away from equilibrium that contrast sharply with predictions derived from the local equilibrium stability analysis.

Fig. 3 shows simulations for a different parameter set, in which the evolutionary cycles observed in Fig. 2*B* occur in a more basic form. These illustrate that the coevolutionary dynamics is dominated alternatingly by inter- and intralocus sexual conflict, with periods of arms races that displace the sexes from their optima, and phases of intralocus sexual conflict resolution that set the stage for the next arms race to occur. Note that the resolution of IASC in these simulations is only partly mediated by the evolution of sexual dimorphism. IASC is also resolved by dynamic changes in the direction of intersexual selection and associated shifts in sex-specific fitness optima, which may temporarily align the selection gradients on correlated characters in males and females. At other times, the same process may cause sex-specific optima to diverge again, leading to the renewed buildup of IASC. Furthermore, a comparison between the panels illustrates that the destabilizing effect of between-sex pleiotropy is trait-specific:

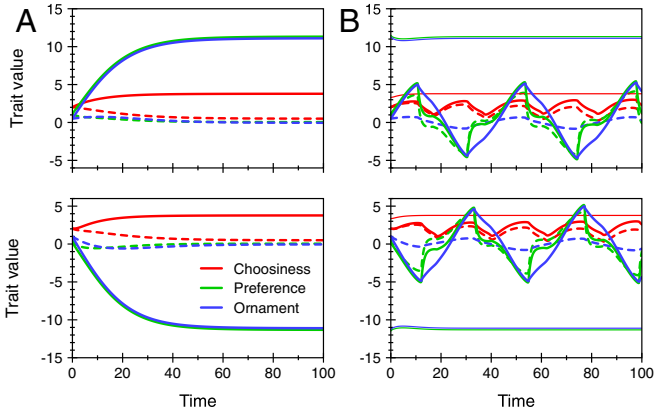

Fig. 2. IASC gives rise to an alternative evolutionary attractor when mating is based on trait complementarity. (*A*) Chase-away sexual selection drives the population toward exaggerated trait values when the intersexual genetic correlations are relatively low ($r_x=r_z=0.5$ and $r_y=0.2$). (*Upper* and *Lower*) Simulations converging on two alternative equilibria. Two additional stable equilibria exist when choosiness is allowed to be negative at equilibrium. We do not show further results for this case, because the evolutionary trajectories at positive and negative values of choosiness are nearly symmetric. Thick lines in *B*, *Upper* and *Lower* show simulations from the same initial conditions as in *A*, but at higher values of the intersexual additive genetic correlation ($r_x=r_z=0.95$ and $r_y=0.2$). Here, males and females engage in arms races, which are reversed halfway on their way toward attaining equilibrium. The cause of these sudden reversals is IASC resolution, which induces a correlated selection response in the mating traits, changing the relative positions of the sexes in their coevolutionary chase. The interaction of inter- and intralocus conflict thus keeps the sexes caught in a perpetual cycle of arms races, alternated by phases of conflict resolution. The equilibrium states attained in *A* are also potential endpoints of evolution in *B* but can only be reached from initial conditions close to the equilibria. This is shown by two example simulations (thin lines) that converge on the alternative equilibria in *B*, *Upper* and *Lower*. Parameters (other than the intersexual correlations) are as in Fig. 1.

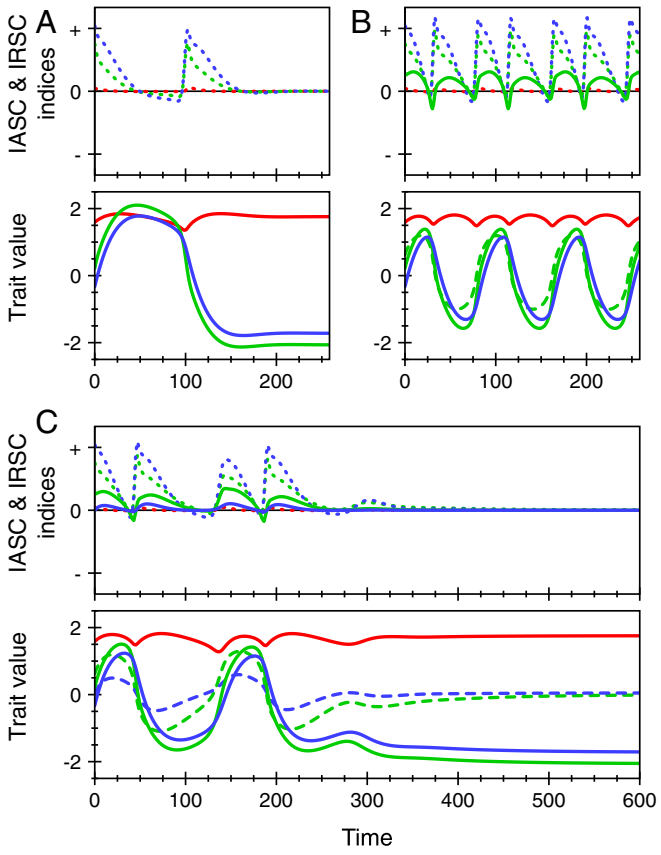

Fig. 3. Effect of between-sex pleiotropy on the dynamics of IASC and IRSC during trait evolution. Each panel shows a simulation of evolving mean trait values (*Lower*; line styles as in Fig. 2) with a corresponding time plot of trait-specific indices of sexually antagonistic selection (dashed: IRSC index; solid: IASC index). Positive values of IASC and IRSC indices are indicative of sexual antagonism; negative values indicate that fitness effects are concordant between the sexes (*Materials and Methods*). (*A*) Complementarity-based mating without between-sex pleiotropy ($r_x = r_y = r_z = 0$). Preference and ornament evolve in an arms race driven by IRSC, first in one then in the other direction, converging eventually on a stable equilibrium. In *B*, the approach to the equilibrium is destabilized by IASC, which can be seen to build up during the period that IRSC is strong ($r_x = 0.8$; $r_y = r_z = 0$). IASC is resolved when x_{σ} evolves back toward it sex-specific optimum, but this process induces a correlated change in x_{φ} that causes the direction of sexual selection to reverse. As a result, a new IRSC arms race is triggered, initially accelerated by concordant selection on the preference and its pleiotropic character. (*C*) When also male ornamentation genes have pleiotropic effects in the other sex ($r_x = 0.8$; $r_y = 0.5$; $r_z = 0$) evolution can attain the equilibrium again. Although the overall level of between-sex pleiotropy and IASC have increased relative to *B*, conflict resolution has become less effective in reversing the direction of sexual selection. This is because both x_{φ} and y_{σ} are pushed toward their viability selection optimum by the correlated response to stabilizing selection on, respectively, x_{σ} and y_{φ}. The difference between the two traits, which determines the direction of chase-away sexual selection, is therefore less strongly affected by IASC resolution than in *B*. Parameters are $a = 0.4$, $b = 0.1$, $\theta_{x_{\varphi}} = \theta_{x_{\sigma}} = 0$, $\theta_{y_{\sigma}} = \theta_{y_{\varphi}} = 0.05$, $\theta_{z_{\varphi}} = 0.95$, $\theta_{\psi} = 0.25$, $c_{x_{\varphi}} = 0.1$, $c_{x_{\sigma}} = c_{y_{\sigma}} = c_{y_{\varphi}} = c_{z_{\varphi}} = 0.05$. For clarity, trait values for the correlated characters and IASC indices are not shown if the corresponding intersexual genetic correlation is equal to zero.

In order for IASC resolution to reverse the direction of chase-away sexual selection (which requires that $x_{\varphi} - y_{\sigma}$ changes sign), the correlated selection response, which pulls the traits back to their viability selection optimum, must be larger in females than in males (*SI Appendix*, Figs. S2–S4).

Global Bifurcation Analysis. The remaining section of the Results provides a description of how the dynamical effects of between-sex pleiotropy unfold, building on insights from dynamical-systems analysis (39). Readers unfamiliar with this subject can first read *Discussion*, where we concentrate on the biological implications of the results.

Because time plots are not well suited to summarize the results of simulations from multiple initial conditions, we switched to a representation of the evolutionary dynamics in phase space and reduced the number of variables to enable visualization of the phase diagrams in 3D. This was accomplished by treating z_{φ} as a fixed character (equivalent to assuming the absence of additive genetic variation in female choosiness) and setting $r_y = r_z = 0$, such that the evolution of y_{φ} and z_{σ} is decoupled from that of the other characters. The remaining characters, x_{φ}, x_{σ}, and y_{σ} appear as variables on the axes of the phase diagrams in Fig. 4. The six panels illustrate the dynamics at different values of the intersexual correlation r_x, increasing from 0.6 in Fig. 4*A* to 0.9 in Fig. 4*F*. In this section, we consider only the model variant with complementarity-based mating.

The phase diagram depicted in Fig. 4*A* reflects qualitatively what we have seen in Fig. 2*A*: Starting from trait values near 0, chase-away sexual selection can occur in two different directions, leading to either one of two stable endpoints (colored red and green) at which males and females express costly mating traits. IASC is fully resolved at these equilibria, with the correlated character x_{σ} being at its viability selection optimum ($\theta_{x_{\sigma}} = 0$). The two attractors are separated by a saddle point (gray), which has a stable manifold that divides the phase space into the separate basins of attraction of the red and the green equilibrium. Intersexual arms races leading toward the stable fixed points exhibit damped oscillations. These have become exaggerated in Fig. 4*B* ($r_x = 0.7$), giving rise to a first bifurcation (i.e., a qualitative change in the phase diagram) that is marked by the appearance of an unstable limit cycle (dotted black). Trajectories leading from the saddle point toward the green equilibrium loop around the cycle, eventually to converge on the red equilibrium. The bias toward the red equilibrium is caused by a slight asymmetry in the viability selection optima for the female preference and the male ornament ($\theta_{x_{\varphi}} = 0$, $\theta_{y_{\sigma}} = 0.05$). As a consequence, the difference between x_{φ} and y_{σ} is smaller in the vicinity of the green equilibrium, making it easier for intralocus sexual conflict resolution to reverse the direction of chase-away sexual selection (*SI Appendix*, Fig. S2). However, at slightly higher values of the intersexual genetic correlation (Fig. 4*C*; $r_x = 0.76$), the approach to the red equilibrium is also destabilized. A second unstable limit cycle has emerged, causing recurrent reversals of the direction of sexually antagonistic coevolution until the process eventually settles down at the red equilibrium.

In Fig. 4*D* ($r_x = 0.8$), a connection between the stable and unstable manifolds of the two limit cycles has led to the appearance of a third cycle (dark blue), which attracts trajectories in the interior of the phase space. The unstable limit cycles now prevent evolution from reaching either one of the stable equilibria, except from a restricted range of initial conditions (comparable to the case illustrated by Fig. 2*B*). When the intersexual correlation is increased even more, two additional bifurcations occur that further restrict the possibility of establishing a truce between the sexes. First, an unstable cycle arises (Fig. 4*E*; $r_x = 0.85$), which acts as a source for trajectories leading to the stable fixed points. This cycle tightly surrounds the saddle point and eventually collapses onto it (Fig. 4*F*; $r_x = 0.9$), transferring its stability properties to the interior equilibrium (gray). It is possible for evolution to reach the stable fixed points from the neighborhood of this equilibrium, following trajectories that spiral outward along the manifold on which the unstable cycle existed. However, selection is much more likely to push the population along the unstable manifold of the former saddle point, which continues to dominate the dynamics around the interior equilibrium. Evolution in this direction very quickly drives the population

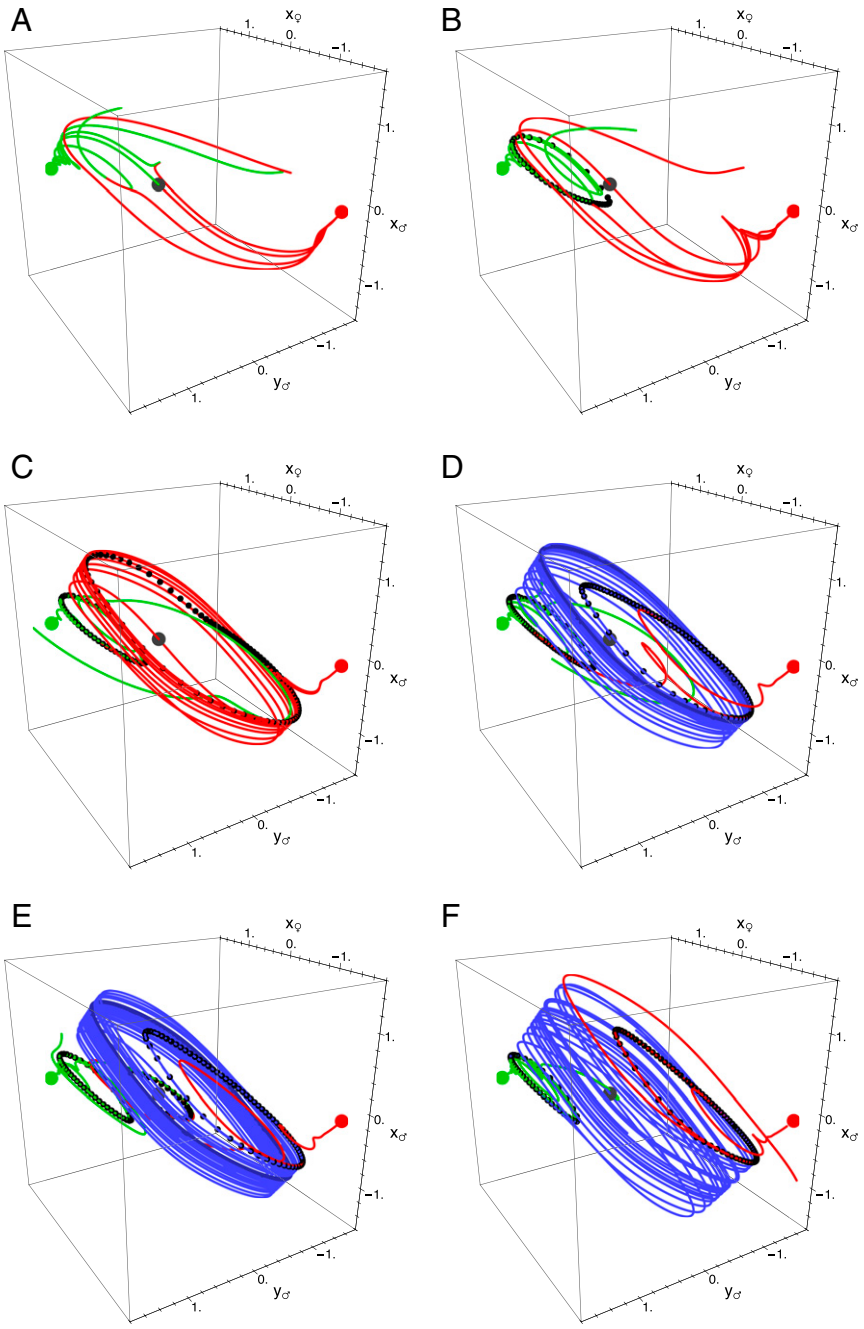

Fig. 4. Between-sex pleiotropy induces a sequence of qualitative changes in the dynamics of sexual conflict. The phase diagrams (*A–F*) show evolutionary trajectories starting from different initial conditions at six different values of the intersexual genetic correlation r_x: (*A*) $r_x = 0.6$, (*B*) $r_x = 0.7$, (*C*) $r_x = 0.76$, (*D*) $r_x = 0.8$, (*E*) $r_x = 0.85$, and (*F*) $r_x = 0.9$. Two stable equilibria (indicated by a red and green dot) exist throughout this range of parameter values, separated by a third, unstable equilibrium (gray dot) in the interior of the trait space. Trajectories are colored according to the attractor at which they end up; differences in line thickness are used to highlight important trajectories. Seen from the upper right, trajectories generally follow a counterclockwise motion. Unstable limit cycles (present in *B–F*) are indicated by black dots. Stable periodic attractors (thick closed orbits in *D–F*) and the trajectories leading toward them are shown in blue. Throughout, female choosiness was kept fixed at $z_♀ = 1.5$, consistent with the absence of genetic variation for that trait. To further reduce the number of variables, we took $r_y = r_z = 0$, so that $y_♀$ and $z_♂$ evolve independently of the other traits. Other parameters are $a = 0.4$, $b = 0.1$, $\theta_{x_♀} = \theta_{x_♂} = 0$, $\theta_{y_♂} = 0.05$, $\theta_\psi = 0.25$, $c_{x_♀} = 0.1$, $c_{x_♂} = c_{y_♂} = 0.05$.

into the basin of attraction of the stable limit cycle, so that continual arms races are a much more likely outcome of evolution.

In this entire series of bifurcations, only the final bifurcation is associated with a change in the qualitative properties of an equilibrium (without even affecting its stability). The other qualitative changes that occurred in the phase diagram result from global bifurcations (*SI Appendix*, Fig. S5) that are not detected by a stability analysis of the equilibria. Moreover, we note that there has not been a single qualitative change in the evolutionary dynamics close to the stable fixed points (red and green) over the entire range of intersexual correlations (Fig. 4).

The above analysis relies on a number of simplifying assumptions, so we ran several checks to verify the robustness of the results. First, we recovered a similar sequence of bifurcations in a model with

coevolving female choosiness (*SI Appendix*, Fig. S6), indicating that the main results are not specific to the reduced model with only three coevolving characters. Another restriction, implicit in our use of a quantitative genetics framework, is that we have assumed a fixed genetic architecture of the traits, whereas, in reality, the genetic variances and covariances are responding to selection (40). In fact, previous studies have shown that IRSC is capable of generating strong linkage equilibria within populations, leading to bimodal trait distributions and possibly speciation (8, 41). However, without high mutation rates and weak selection on females, phenotypic diversification is limited in individual-based simulations of our model (*SI Appendix*, Figs. S7–S12). Despite being genetically explicit (enabling the genetic architecture of traits to evolve), the individual-based simulations closely follow the quantitative genetic predictions, lending support to the robust occurrence of the instability uncovered by our analysis.

Discussion

The potential for IASC to affect trait evolution and diversification caused by IRSC has recently been emphasized (4) but never before put to the test of formal analysis. Previous models of IRSC (7, 8, 10, 32, 33), which have not included IASC, predict arms races of sexually antagonistic adaptation and counteradaptation between the sexes, possibly leading to exaggerated traits and substantial fitness losses due to sexual conflict (6). We included IASC in a quantitative genetic model of IRSC trait evolution and found that, depending on the genetic architecture of traits (i.e., their degree of sex-limited expression) and the biological mechanism of mating interactions (i.e., whether compatibility is determined by a contest or trait complementarity), IASC can either restrain or induce male–female antagonistic coevolution.

The stabilizing effect of IASC dominates near evolutionary equilibria. Here, selection is weak and trait values evolve slowly, so that there is ample time for the resolution of IASC. Because the correlated characters are close to their optimum, mutations expressed in mating interactions are also exposed to purifying selection in the other sex. A general mathematical argument confirms that this additional source of stabilizing selection thwarts the initiation of arms races in populations at evolutionary equilibrium.

Far away from equilibrium, the mating traits evolve more rapidly, allowing unresolved IASC to build up. The pleiotropic effect of mating-trait mutations is then subject to directional selection in the other sex, which can slow down antagonistic coevolution, or even reverse its direction. The latter phenomenon occurs with complementarity-based mating, when the female preference, which is ahead in the coevolutionary chase, is subject to stronger pleiotropic constraints than the male ornament, which is following behind (*SI Appendix*, Figs. S2–S4). Furthermore, arms-race reversals occur above a critical level of the intersexual correlation, at which the correlated selection response to IASC resolution is sufficient to pull the mean female preference toward the other side of the male trait distribution, qualitatively changing the direction of chase-away sexual selection. In this way, rather than helping the sexes to maintain a truce, IASC fuels a never-ending cycle of IRSC arms races, interrupted by phases of IASC resolution, which set the stage for the next arms race to occur.

In conclusion, whether IASC stabilizes or destabilizes IRSC arms races is determined primarily by the balance between the rate of conflict resolution and the rate at which new sexually antagonistic variation is accumulated during episodes of rapid trait evolution. The timescale of both processes is affected by the genetic architecture of conflict traits, characterized in our analysis by the additive genetic intersexual correlation between mating characters and their pleiotropic homologs in the other sex. Research that has focused solely on IASC has shown that negative intersexual correlations for fitness are maintained in populations (11, 19, 26), suggesting that the resolution of IASC may be slow (20, 22) (but see ref. 42). However, intersexual genetic correlations for individual traits are varied (19), with systematic differences existing among trait types (20). Moreover, specific information on the extent of between-sex pleiotropy for traits involved in IRSC is scarce. Quantitative estimates of the strength of interaction between IASC and IRSC therefore require further developments in our understanding of the genetic basis of the two forms of sexual conflict.

The Genetic Architecture of Sexual Conflict. Currently, the most detailed studies of the genetics of IRSC come from seminal proteins. Sex peptide (SP) is one gene that has been recognized as a mediator of IRSC (15), and other candidate genes have also been identified, including genes that are required by females to respond to SP postmating (25, 37). Several IRSC candidate genes identified by Gioti et al. (37) were not sex-limited in their expression, creating potential for them to also mediate IASC. Similarly, Innocenti and Morrow (30) found that many of the transcripts associated with IASC were enriched in reproductive tissues, such as the female spermatheca and the male accessory gland and ejaculatory duct. Altogether, this suggests that the same loci could be involved in both IASC and IRSC.

Although reproductive traits are the primary candidates to mediate both types of sexual conflict, sexually antagonistic transcripts associated with IASC have also been identified in nonreproductive tissues (30), and several aspects of morphology and physiology that are exposed to sex-specific selection but not directly related to reproductive functions have strong genetic correlations between the sexes (20). Nonreproductive traits may also be necessary to counteradapt in an IRSC arms race. For example, in cockroaches and bed bugs, behavioral, morphological, and physiological adaptations are thought to be involved in adaptations to IRSC in both sexes (16, 33). Nonreproductive traits may therefore participate in both IRSC and IASC, although reproductive traits might generally be subject to stronger sex-specific selection.

Estimating between-sex genetic correlations is a challenge, because correlated phenotypic characters can easily be overlooked due to the diffuse nature of pleiotropy. Therefore, a promising complementary approach to genomic analyses of the genetic architecture of sexual conflict traits is to test for IASC effects using experimental manipulations of candidate genes previously identified for their role in sexually antagonistic interactions. It might also be insightful to conduct artificial selection experiments on traits involved in IRSC, to identify whether the traits have a shared genetic basis, where resulting phenotypes and their fitness effects could be quantified in each sex. A recent study by Fuchikawa and Okada (43) used this method to study whether exaggeration of male mandibles in seed beetles affected female fitness via an intersexual genetic correlation. Although they found no evidence of IASC over this trait, it provides a framework for other studies of this kind.

Mechanisms of Mating Interactions. Apart from between-sex pleiotropy, a requirement for sustained arms-race reversals in our model is that mating compatibility is determined by trait complementarity rather than by a contest between offense and defense traits. IASC was observed to complicate the dynamics of arms races in the contest scenario as well (*SI Appendix*, Fig. S1), but its destabilizing effects never prevented evolution from ultimately reaching an equilibrium state. Both mating mechanisms have been considered in theoretical studies of IRSC and motivated by specific biological examples (8). RCD05 already showed that evolutionary cycles, featuring fluctuations in sensitivity (Fig. 1 and *SI Appendix*, Fig. S1), may occur when mating is determined by a contest. However, barring changes in sensitivity, changing the direction of chase-away sexual selection is precluded in the contest model, because male sexual fitness is an increasing function of the expression of the offense trait, irrespective of the level of female defense. A similar monotonic relationship holds for female sexual fitness as a function of the defense trait. These

constraints, however, are an immediate consequence of the assumption that offense and defense are unidimensional traits.

Male and female mating behaviors are frequently determined by many traits (including behavioral, morphological, and physiological characteristics). Accordingly, intersexual arms races generally occur in multidimensional phenotype space. There, male–female coevolution can unfold in many different directions, so that the resolution of IASC may trigger sudden changes in the direction of arms races. Populations evolving in multidimensional phenotype spaces, in which mating interactions are governed by a contest between more than one offense and defense trait, may therefore show complex dynamics of sexual conflict similar to what is observed in our model for complementarity-based mating. Consistent with this hypothesis, frequency-dependent selection operating on multivariate phenotypes is known to frequently result in complex nonequilibrium dynamics or even evolutionary chaos (44).

Implications for Theory. The evolutionary cycling observed in our model of sexual conflict is a consequence of an interaction between processes on a fast and a slow timescale, typical of systems with delayed nonlinear feedback control [relaxation oscillators (45)]. Sexually antagonistic coevolution is the fast process (7), which drags along pleiotropically correlated characters. The accumulating displacement of these characters from their optimum acts as a control variable with a sudden, switch-like effect on the direction of intersexual selection, mediated by IASC resolution. The strength of the feedback and its timescale of operation are set by the additive genetic correlations. Broadening this analogy, we speculate that similar dynamical instabilities can occur in other coevolutionary processes that are subject to pleiotropic constraints, such as in the context of host–parasite coevolution (6) or biological signaling (46). Because pleiotropy has been seen predominantly as a source of evolutionary constraint so far, further theoretical investigation into its consequences for the dynamics of evolution is warranted.

The rich dynamics of sexual conflict, uncovered by a numerical bifurcation analysis, also draws the attention to the limitations of equilibrium analyses to characterize complex evolutionary phenomena. The standard approach to analyzing phenotypic models of evolution is to locate evolutionary equilibria and then characterize their stability by studying the dynamics of evolution in the vicinity of the equilibria (47). This local analysis does not provide conclusive information about the dynamics far away from equilibria, yet its results are often extrapolated to infer a qualitative description of the global evolutionary dynamics. The present model serves as an illustration of a biological scenario where such qualitative analysis leads to the wrong conclusions. Specifically, the analytical results fail to detect the emergence of an evolutionary cycle that arises through a series of global bifurcations and serves as an alternative evolutionary attractor. How commonly this problem occurs in the analysis of biological models is an open question, especially for studies of complex trait evolution, because a systematic search for global bifurcations is not routinely included in model analyses.

Conclusion

Our findings inspire an integrative perspective on the biology of inter- and intrasexual conflict that sheds new light on several issues debated in the field. First, we show that pleiotropic constraints, in the form of correlated trait expression subject to stabilizing selection, do not necessarily restrain arms races but may rather create conditions favorable to perpetual antagonistic coevolution. The reversal of arms races by IASC resolution provides a previously unidentified mechanism for explaining the ongoing evolution of mating traits, despite the presence of stabilizing natural selection preventing unlimited trait exaggeration. Second, our simulations, which show a recurrent buildup of unresolved IASC during intersexual arms races, alternated by periods of conflict resolution, suggest that IASC may be more dynamic than has so far been recognized. This idea is consistent with the observation that closely related species show markedly different patterns of sex-biased gene expression (42). It can also help to resolve the paradox that appreciable levels of sexually antagonistic genetic variation segregate in populations, whereas sexual dimorphism is known to evolve rapidly in many cases (12, 22, 48). That is, even if the evolution of sexual dimorphism leads to a rapid loss of sexually antagonistic variation, new sexually antagonistic alleles might be introduced continually as a pleiotropic side-effect of intersexual arms races.

Materials and Methods

Fitness Functions. Individual fitness is calculated as the product of survival and reproductive success. Reproductive success depends on the mating rate ψ in both sexes, but in qualitatively different ways: Male fitness is an increasing function of ψ, whereas female fitness is maximized at an intermediate mating rate θ_ψ. Male and female survival are affected similarly by stabilizing natural selection, which acts independently on each of the phenotypic characters expressed by the individual. Hence, the fitness of a female is a function of her own phenotype ($x_♀, y_♀$, and $z_♀$) and of her mating rate, which also depends on the average persistence $\bar{y}_♂$ of the resident males with whom she interacts:

$$W_♀ = e^{-\frac{1}{2}a\left(\psi(z_♀(\bar{y}_♂ - x_♀)) - \theta_\psi\right)^2} \times e^{-\frac{1}{2}\left(c_{x_♀}\left(x_♀ - \theta_{x_♀}\right)^2 + c_{y_♀}\left(y_♀ - \theta_{y_♀}\right)^2 + c_{z_♀}\left(z_♀ - \theta_{z_♀}\right)^2\right)}. \quad [2]$$

Likewise, the fitness of a male depends on his own traits $x_♂$, $y_♂$, and $z_♂$, and on the average threshold $\bar{x}_♀$ and sensitivity $\bar{z}_♀$ of his mating partners:

$$W_♂ = e^{b\,\psi(\bar{z}_♀(y_♂ - \bar{x}_♀))} \times e^{-\frac{1}{2}\left(c_{x_♂}\left(x_♂ - \theta_{x_♂}\right)^2 + c_{y_♂}\left(y_♂ - \theta_{y_♂}\right)^2 + c_{z_♂}\left(z_♂ - \theta_{z_♂}\right)^2\right)}. \quad [3]$$

In these expressions, the parameters a and b scale the fitness consequences to females and males of IRSC. Moreover, θ_k and c_k (where k can stand for any of the phenotypic characters) specify the optimal value of character k under natural selection and the stabilizing selection intensity, respectively.

Calculating the Response to Selection. The strength and direction of selection on the phenotypic characters is quantified by the selection gradient, $\boldsymbol{\beta} = (\beta_{x_♀}, \beta_{z_♀}, \beta_{y_♂}, \beta_{x_♂}, \beta_{z_♂}, \beta_{y_♀})^T$. Its elements are calculated directly from the fitness functions (Eqs. **2** and **3**), using standard methods from evolutionary quantitative genetics (49). Specifically, depending on whether k is expressed in females or males,

$$\beta_k = \left.\frac{d \ln W_♀}{d\, k}\right|_{\substack{x_♀ = \bar{x}_♀ \\ y_♀ = \bar{y}_♀ \\ z_♀ = \bar{z}_♀}} \text{ or } \left.\frac{d \ln W_♂}{d\, k}\right|_{\substack{x_♂ = \bar{x}_♂ \\ y_♂ = \bar{y}_♂ \\ z_♂ = \bar{z}_♂}}.$$

In the calculation of the selection gradients, we follow the common approach of assuming weak selection and limited phenotypic variation in the population. On the scale of a phenotypic SD, the fitness function can then be approximated by a linear function, and the selection gradients become independent of the phenotypic variances. Qualitatively different outcomes of sexual conflict occur in populations with high levels of standing genetic variation, in which case the approximations underlying Eq. **1** break down (*SI Appendix, Individual-based simulations*).

The population average value of each character changes in response to selection acting on the character itself, and due to selection on correlated characters. The combined effect of the direct and indirect component of the selection response is found by multiplying the selection gradient with the genetic variance–covariance matrix **G** (38). Several of the off-diagonal elements of **G** represent additive genetic covariances between a mating character and its pleiotropic character in the other sex (2). These intersexual covariances are of prime interest, because they quantify to what extent the resolution of IASC is constrained by male and female traits sharing a common genetic basis. The other off-diagonal elements measure covariance between nonhomologous characters due to pleiotropy or linkage disequilibrium. For simplicity, these elements of **G** are assumed to be negligibly small.

The number of parameters can be reduced further, if all traits are measured on a standardized scale. In that case, the additive genetic variances are equal to one and **G** takes the form of a correlation matrix:

$$\mathbf{G} = \begin{pmatrix} 1 & 0 & 0 & r_x & 0 & 0 \\ 0 & 1 & 0 & 0 & r_z & 0 \\ 0 & 0 & 1 & 0 & 0 & r_y \\ r_x & 0 & 0 & 1 & 0 & 0 \\ 0 & r_z & 0 & 0 & 1 & 0 \\ 0 & 0 & r_y & 0 & 0 & 1 \end{pmatrix}. \quad [4]$$

Here, r_x, r_y, and r_z denote the additive genetic intersexual correlations between the expression of a mating character in one sex and its homologous pleiotropic character in the other.

Quantifying IASC and IRSC. Following ref. 19, we consider IASC to arise when the selection gradients on genetically correlated characters in males and females point in opposite directions. The indices of IASC plotted in Fig. 3 and *SI Appendix*, Fig. S1 are therefore calculated as

$$I_x^{\mathrm{IASC}} = -\beta_{x_♀}\,\beta_{x_♂},\ I_y^{\mathrm{IASC}} = -\beta_{y_♀}\,\beta_{y_♂} \text{ and } I_z^{\mathrm{IASC}} = -\beta_{z_♀}\,\beta_{z_♂}.$$

Comparable indices for the strength of IRSC are calculated by multiplying the selection gradient of a mating trait with its effect on fitness in the other sex, that is:

$$I_x^{\mathrm{IRSC}} = -\beta_{x_♀}\frac{d\ln W_♂}{d\,\bar{x}_♀} = b\,\beta_{x_♀}\,\bar{z}_♀\,\bar{\psi}',$$

$$I_y^{\mathrm{IRSC}} = -\beta_{y_♂}\frac{d\ln W_♀}{d\,\bar{y}_♂} = a\,\beta_{y_♂}\,\bar{z}_♀\,(\bar{\psi}-\theta_\psi)\,\bar{\psi}',$$

$$I_z^{\mathrm{IRSC}} = -\beta_{z_♀}\frac{d\ln W_♂}{d\,\bar{z}_♀} = b\,\beta_{z_♀}\,(\bar{x}_♀-\bar{y}_♂)\,\bar{\psi}'.$$

ACKNOWLEDGMENTS. The authors thank Leonardo Oña, Andrés Quiñones, and two anonymous reviewers for their constructive comments on the manuscript. This work was supported by Starting Independent Researcher Grant 309555 of the European Research Council and Vidi Grant 864.11.012 of the Netherlands Organization for Scientific Research (to G.S.v.D.) and by European Research Council Starting Grant 280632 and the Royal Society University Research Fellowship scheme (to T.M.P. and E.H.M.).

1. Parker GA (1979) Sexual selection and sexual conflict. *Sexual Selection and Reproductive Competition in Insects*, eds Blum MS, Blum NA (Academic, New York), pp 123–166.
2. Lande R (1980) Sexual dimorphism, sexual selection, and adaptation in polygenic characters. *Evolution* 34(2):292–305.
3. Hosken DJ, Stockley P (2004) Sexual selection and genital evolution. *Trends Ecol Evol* 19(2):87–93.
4. Pennell TM, Morrow EH (2013) Two sexes, one genome: The evolutionary dynamics of intralocus sexual conflict. *Ecol Evol* 3(6):1819–1834.
5. Parker GA, Partridge L (1998) Sexual conflict and speciation. *Phil Trans R Soc B Biol Sci* 353(1366):261–274.
6. Rice W, Holland B (1997) The enemies within: Intergenomic conflict, interlocus contest evolution (ICE), and the intraspecific Red Queen. *Behav Ecol Sociobiol* 41(1):1–10.
7. Gavrilets S (2000) Rapid evolution of reproductive barriers driven by sexual conflict. *Nature* 403(6772):886–889.
8. Gavrilets S (2014) Is sexual conflict an "engine of speciation"? *Cold Spring Harb Perspect Biol* 6(12):a017723.
9. Holland B, Rice W (1998) Chase-away sexual selection: Antagonistic seduction versus resistance. *Evolution* 52(1):1–7.
10. Gavrilets S, Arnqvist G, Friberg U (2001) The evolution of female mate choice by sexual conflict. *Proc R Soc B Biol Sci* 268(1466):531–539.
11. Brommer JE, Kirkpatrick M, Qvarnström A, Gustafsson L (2007) The intersexual genetic correlation for lifetime fitness in the wild and its implications for sexual selection. *PLoS One* 2(8):e744.
12. van Doorn GS (2009) Intralocus sexual conflict. *Ann N Y Acad Sci* 1168:52–71.
13. Arnqvist G, Rowe L (1995) Sexual conflict and arms races between the sexes: A morphological adaptation for control of mating in a female insect. *Proc R Soc B Biol Sci* 261(1360):123–127.
14. Koene JM, Schulenburg H (2005) Shooting darts: Co-evolution and counter-adaptation in hermaphroditic snails. *BMC Evol Biol* 5:25.
15. Wigby S, Chapman T (2005) Sex peptide causes mating costs in female Drosophila melanogaster. *Curr Biol* 15(4):316–321.
16. Reinhardt K, Naylor R, Siva-Jothy MT (2003) Reducing a cost of traumatic insemination: Female bedbugs evolve a unique organ. *Proc Biol Sci* 270(1531):2371–2375.
17. Rice WR (1984) Sex chromosomes and the evolution of sexual dimorphism. *Evolution* 38(4):735–742.
18. Bonduriansky R, Chenoweth SF (2009) Intralocus sexual conflict. *Trends Ecol Evol* 24(5):280–288.
19. Cox RM, Calsbeek R (2009) Sexually antagonistic selection, sexual dimorphism, and the resolution of intralocus sexual conflict. *Am Nat* 173(2):176–187.
20. Poissant J, Wilson AJ, Coltman DW (2010) Sex-specific genetic variance and the evolution of sexual dimorphism: A systematic review of cross-sex genetic correlations. *Evolution* 64(1):97–107.
21. Wyman MJ, Stinchcombe JR, Rowe L (2013) A multivariate view of the evolution of sexual dimorphism. *J Evol Biol* 26(10):2070–2080.
22. Stewart AD, Pischedda A, Rice WR (2010) Resolving intralocus sexual conflict: Genetic mechanisms and time frame. *J Hered* 101(Suppl 1):S94–S99.
23. Gosden TP, Shastri KL, Innocenti P, Chenoweth SF (2012) The B-matrix harbors significant and sex-specific constraints on the evolution of multicharacter sexual dimorphism. *Evolution* 66(7):2106–2116.
24. Griffin RM, Dean R, Grace JL, Rydén P, Friberg U (2013) The shared genome is a pervasive constraint on the evolution of sex-biased gene expression. *Mol Biol Evol* 30(9):2168–2176.
25. Ingleby FC, Innocenti P, Rundle HD, Morrow EH (2014) Between-sex genetic covariance constrains the evolution of sexual dimorphism in Drosophila melanogaster. *J Evol Biol* 27(8):1721–1732.
26. Foerster K, et al. (2007) Sexually antagonistic genetic variation for fitness in red deer. *Nature* 447(7148):1107–1110.
27. Mainguy J, Côté SD, Festa-Bianchet M, Coltman DW (2009) Father-offspring phenotypic correlations suggest intralocus sexual conflict for a fitness-linked trait in a wild sexually dimorphic mammal. *Proc R Soc B Biol Sci* 276(1675):4067–4075.
28. Chippindale AK, Gibson JR, Rice WR (2001) Negative genetic correlation for adult fitness between sexes reveals ontogenetic conflict in Drosophila. *Proc Natl Acad Sci USA* 98(4):1671–1675.
29. Bedhomme S, Prasad NG, Jiang PP, Chippindale AK (2008) Reproductive behaviour evolves rapidly when intralocus sexual conflict is removed. *PLoS One* 3(5):e2187.
30. Innocenti P, Morrow EH (2010) The sexually antagonistic genes of Drosophila melanogaster. *PLoS Biol* 8(3):e1000335.
31. Hesketh J, Fowler K, Reuter M (2013) Genetic drift in antagonistic genes leads to divergence in sex-specific fitness between experimental populations of Drosophila melanogaster. *Evolution* 67(5):1503–1510.
32. Rowe L, Cameron E, Day T (2005) Escalation, retreat, and female indifference as alternative outcomes of sexually antagonistic coevolution. *Am Nat* 165(Suppl 5):S5–S18.
33. Moore AJ, Pizzari T (2005) Quantitative genetic models of sexual conflict based on interacting phenotypes. *Am Nat* 165(Suppl 5):S88–S97.
34. Gibson J, Chippindale AK, Rice WR (2002) The X chromosome is a hot spot for sexually antagonistic fitness variation. *Proc R Soc B Biol Sci* 269(1490):499–505.
35. Andrés JA, Morrow EH (2003) The origin of interlocus sexual conflict: Is sex-linkage important? *J Evol Biol* 16(2):219–223.
36. Rice WR, et al. (2005) Inter-locus antagonistic coevolution as an engine of speciation: Assessment with hemiclonal analysis. *Proc Natl Acad Sci USA* 102(Suppl 1):6527–6534.
37. Gioti A, et al. (2012) Sex peptide of Drosophila melanogaster males is a global regulator of reproductive processes in females. *Proc R Soc B Biol Sci* 279(1746):4423–4432.
38. Lande R, Arnold SJ (1983) The measurement of selection on correlated characters. *Evolution* 37(6):1210–1226.
39. Kuznetsov Y (2004) *Elements of Applied Bifurcation Analysis* (Springer, New York).
40. Kirkpatrick M, Johnson T, Barton N (2002) General models of multilocus evolution. *Genetics* 161(4):1727–1750.
41. Gavrilets S, Waxman D (2002) Sympatric speciation by sexual conflict. *Proc Natl Acad Sci USA* 99(16):10533–10538.
42. Ranz JM, Castillo-Davis CI, Meiklejohn CD, Hartl DL (2003) Sex-dependent gene expression and evolution of the Drosophila transcriptome. *Science* 300(5626):1742–1745.
43. Fuchikawa T, Okada K (2013) Inter- and intrasexual genetic correlations of exaggerated traits and locomotor activity. *J Evol Biol* 26(9):1979–1987.
44. Doebeli M, Ispolatov I (2014) Chaos and unpredictability in evolution. *Evolution* 68(5):1365–1373.
45. Van der Pol B (1940) Biological rhythms considered as relaxation oscillations Act. *Med Scand* 103(S108):76–88.
46. van Doorn GS, Weissing FJ (2006) Sexual conflict and the evolution of female preferences for indicators of male quality. *Am Nat* 168(6):742–757.
47. Otto SP, Day T (2007) *A Biologist's Guide to Mathematical Modeling in Ecology and Evolution* (Princeton Univ Press, Princeton).
48. Badyaev AV (2002) Growing apart: An ontogenetic perspective on the evolution of sexual size dimorphism. *Trends Ecol Evol* 17(8):369–378.
49. Iwasa Y, Pomiankowski A, Nee S (1991) The evolution of costly mate preferences II. The 'handicap' principle. *Evolution* 45(6):1431–1442.

Supporting a truce, while fueling the arms race: contrasting effects of intralocus sexual conflict on sexually antagonistic coevolution — SI Appendix —

Tanya M. Pennell[1], Freek J.H. de Haas[2], Edward H. Morrow[1], and G. Sander van Doorn*[2]

[1] *School of Life Sciences, University of Sussex, United Kingdom*
[2] *Groningen Institute for Evolutionary Life Sciences, University of Groningen, the Netherlands*

This online appendix contains a step-by-step derivation of the general mathematical results (supported by table S1), followed by supplementary figure S1 (dynamic of IASC and IRSC indices in the contest mating scenario), figures S2–S4 (detailing the mechanism of arms-race reversals), figure S5 (schematic representation of global bifurcations), figure S6 (results for a model with coevolving female choosiness) and figures S7–S12 (individual-based simulation results).

Mathematical analysis

Evolutionary equilibria. The point of departure of the mathematical analysis is the multivariate breeder's equation [1]

$$\frac{d\mathbf{u}}{dt} = \mathbf{G}\,\boldsymbol{\beta}(\mathbf{u}), \tag{S1}$$

which describes the evolutionary dynamic of the average trait values. Except in degenerate cases ($r_k = 1$ or $r_k = -1$ for at least one of the traits), which we exclude in the further analysis, the genetic variance-covariance matrix $\mathbf{G}$ is non-singular. This means that $\mathbf{G}^{-1}$ exists, so that the equilibrium points of the system of ordinary differential equations [S1] can be found by solving $\boldsymbol{\beta}(\mathbf{u}^*) = 0$ for the equilibrium trait values $\mathbf{u}^* = (x_♀^*, z_♀^*, y_♂^*, x_♂^*, z_♂^*, y_♀^*)^{\mathrm{T}}$. As a further consequence, neither the number of equilibria nor their location are affected by the genetic variance-covariance matrix.

It follows straightforwardly from equation [1] that $x_♂^*$, $z_♂^*$ and $y_♀^*$ are given by their respective optimal trait values $\theta_{x_♂}$, $\theta_{z_♂}$ and $\theta_{y_♀}$. The equilibrium values of the three remaining characters can be expressed as functions of the mating stimulus $\bar{s}$:

$$\begin{pmatrix} x_♀^*(\bar{s}) \\ z_♀^*(\bar{s}) \\ y_♂^*(\bar{s}) \end{pmatrix} = \begin{pmatrix} c_{x_♀} & -a\,(\psi(\bar{s}) - \theta_\psi)\,\psi'(\bar{s}) & 0 \\ -a\,(\psi(\bar{s}) - \theta_\psi)\,\psi'(\bar{s}) & c_{z_♀} & a\,(\psi(\bar{s}) - \theta_\psi)\,\psi'(\bar{s}) \\ 0 & -b\,\psi'(\bar{s}) & c_{y_♂} \end{pmatrix}^{-1} \begin{pmatrix} c_{x_♀}\theta_{x_♀} \\ c_{z_♀}\theta_{z_♀} \\ c_{y_♂}\theta_{y_♂} \end{pmatrix} \tag{S2}$$

Based on this result, the equilibria can be found by locating the roots of the function $f(\bar{s}) = z_♀^*(\bar{s})\,(y_♂^*(\bar{s}) - x_♀^*(\bar{s})) - \bar{s}$. The equilibrium condition $f(s^*) = 0$ cannot be solved analytically, except in a number of special cases discussed in [2]. However, plotting the graph of f provides a straightforward graphical method to determine how many equilibria there are, while numerical root-finding methods can be applied to approximate the equilibrium values of the mating stimulus to arbitrary precision.

Stability analysis. The stability of the equilibria is assessed by linearizing equation [S1] around each of the equilibrium points,

$$\frac{d(\mathbf{u} - \mathbf{u}^*)}{dt} \approx \underbrace{\mathbf{G}\,\frac{\partial \boldsymbol{\beta}(\mathbf{u})}{\partial \mathbf{u}}\bigg|_{\mathbf{u}=\mathbf{u}^*}}_{\mathbf{M}} (\mathbf{u} - \mathbf{u}^*) \tag{S3}$$

and evaluating the eigenvalues of the matrix $\mathbf{M}$. This matrix, which is the product of the genetic variance-covariance matrix and the Jacobian of the selection gradient, can be written as a block matrix

$$\mathbf{M} = \begin{pmatrix} \mathbf{I} & \mathbf{R} \\ \mathbf{R} & \mathbf{I} \end{pmatrix} \begin{pmatrix} \mathbf{J} & \mathbf{0} \\ \mathbf{0} & -\mathbf{C} \end{pmatrix} = \begin{pmatrix} \mathbf{J} & -\mathbf{RC} \\ \mathbf{RJ} & -\mathbf{C} \end{pmatrix} \tag{S4}$$

where $\mathbf{I}$ is the 3×3 identity matrix, $\mathbf{0}$ is a 3×3 matrix of zeros, and $\mathbf{C}$ and $\mathbf{R}$ are diagonal matrices

$$\mathbf{C} = \begin{pmatrix} c_{x_♂} & 0 & 0 \\ 0 & c_{z_♂} & 0 \\ 0 & 0 & c_{y_♀} \end{pmatrix} \text{ and } \mathbf{R} = \begin{pmatrix} r_x & 0 & 0 \\ 0 & r_z & 0 \\ 0 & 0 & r_y \end{pmatrix} \tag{S5}$$

*Corresponding author; Electronic address: g.s.van.doorn@rug.nl

Table S1. Summary of notation used in the mathematical analysis

Notation	Definition
	Complex numbers[1]
$z \in \mathbb{C}$	Complex number $z = a + i\,b$, where i is the imaginary unit, defined by $i^2 = -1$
$\Re(z)$	Real part of z; $\Re(a + i\,b) = a$
$\Im(z)$	Imaginary part of z; $\Im(a + i\,b) = b$
$\bar{z}$	Complex conjugate of z, i.e., if $z = a + i\,b$ then $\bar{z} = a - i\,b$
$\lvert z\rvert$	Absolute value or magnitude of z, i.e., if $z = a + i\,b$ then $\lvert z\rvert = \sqrt{a^2 + b^2}$
	Vectors and matrices
$\mathbf{x}$	Lowercase boldface symbols represent (column) vectors
$\mathbf{x}_{[i]}$	The number at position i in vector $\mathbf{x}$
$\mathbf{x}^{\mathrm{T}}$	Transpose of a vector; transposition changes column vectors into row vectors and vice versa
$\mathbf{x}^{\dagger}$	Conjugate transpose of a vector; $\mathbf{x}^{\dagger} = \bar{\mathbf{x}}^{\mathrm{T}}$
$\langle \mathbf{x}, \mathbf{y} \rangle$	Inner product of $\mathbf{x}$ and $\mathbf{y}$; $\langle \mathbf{x}, \mathbf{y} \rangle = \mathbf{x}^{\dagger}\mathbf{y} = \sum_k \bar{\mathbf{x}}_{[k]}\mathbf{y}_{[k]}$
$\lVert \mathbf{x} \rVert$	Lenght of $\mathbf{x}$; $\lVert \mathbf{x} \rVert = \sqrt{\langle \mathbf{x}, \mathbf{x} \rangle}$
$\mathbf{A}$	Uppercase boldface symbols represent matrices
$\mathbf{A}_{[i,j]}$	The element at row i and column j of matrix $\mathbf{A}$
$\mathbf{A}^{\mathrm{T}}$	Transpose of a matrix; $\mathbf{A}^{\mathrm{T}}_{[i,j]} = \mathbf{A}_{[j,i]}$
$\mathbf{A}^{\dagger}$	Conjugate transpose of a matrix; $\mathbf{A}^{\dagger} = \bar{\mathbf{A}}^{\mathrm{T}}$
$\mathbf{A}^{\mathrm{S}}$	Symmetric part of matrix $\mathbf{A}$; $\mathbf{A}^{\mathrm{S}} = \frac{1}{2}(\mathbf{A} + \mathbf{A}^{\dagger})$
$\Lambda_{\max}(\mathbf{H})$, $\Lambda_{\min}(\mathbf{H})$	Largest and smallest eigenvalue of a Hermitian[2] matrix $\mathbf{H}$

[1] Definitions in this part of the table assume that $a, b \in \mathbb{R}$
[2] A matrix $\mathbf{H}$ is Hermitian if $\mathbf{H} = \mathbf{H}^{\dagger}$

Throughout, we assume that $0 < r_k < 1$ and $c_k > 0$ for all characters, so that the eigenvalues of $\mathbf{R}^2$, $\mathbf{I} - \mathbf{R}^2$ and $\mathbf{C}$ are strictly positive. Finally, the matrix $\mathbf{J}$, given by

$$\mathbf{J} = \begin{pmatrix} -a\,z_{♀}^{*2}\,\Psi'' - c_{x_{♀}} & a\,\Psi' + a\,s^*\Psi'' & a\,z_{♀}^{*2}\,\Psi'' \\ a\,\Psi' + a\,s^*\Psi'' & -a\,(y_{♂}^* - x_{♀}^*)^2\,\Psi'' - c_{z_{♀}} & -a\,\Psi' - a\,s^*\Psi'' \\ -b\,z_{♀}^{*2}\,\psi''(s^*) & b\,\psi'(s^*) + b\,s^*\psi''(s^*) & b\,z_{♀}^{*2}\,\psi''(s^*) - c_{y_{♂}} \end{pmatrix} \tag{S6}$$

is a 3×3 submatrix of the Jacobian that specifies how small perturbations of $x_{♀}$, $z_{♀}$ or $y_{♂}$ away from their equilibrium value influence the strength and the direction of selection acting on each of the mating characters. Here, we used the shorthand notation $\Psi' = \psi'(s^*)\,(\psi(s^*) - \theta_{\psi})$ and $\Psi'' = \psi''(s^*)\,(\psi(s^*) - \theta_{\psi}) + \psi'(s^*)^2$. Furthermore, $s^* = z_{♀}^* \times (y_{♂}^* - x_{♀}^*)$ denotes the equilibrium value of the mating stimulus. Aside from the contributions of stabilizing natural selection that appear on the diagonal, $\mathbf{J}$ captures the fitness consequences of IRSC, which are mediated by the effects of the mating characters on the value of the mating stimulus.

The equilibrium is stable if and only if all eigenvalues of $\mathbf{M}$ have negative real parts. Accordingly, if λ is the eigenvalue with the largest real part, a necessary and sufficient condition for stability is that $\Re(\lambda) < 0$ (a summary of our notation used for complex numbers is provided in table S1). Let $\mathbf{w}$ be the eigenvector associated with eigenvalue λ. In accordance with the block structure of $\mathbf{M}$, $\mathbf{w}$ is split into two parts, which are written as linear combinations of two vectors $\mathbf{u}, \mathbf{v} \in \mathbb{C}^3$. We are primarily interested in the case that $\Re(\lambda) > 0$ for $\mathbf{R} \to \mathbf{I}$, implying that the equilibrium is not stable in the absence of intersexual genetic correlations, (and aim to show that such an equilibrium can become stable for some $\mathbf{R} \neq \mathbf{I}$). In this case, $\mathbf{J}$ has at least one eigenvalue with positive real part. The further calculations simplify if we choose

$$\mathbf{w} = \begin{pmatrix} \mathbf{u} + \mathbf{R}\mathbf{v} \\ \mathbf{v} \end{pmatrix}, \text{ such that } \mathbf{M}\mathbf{w} = \lambda\mathbf{w} \;\Leftrightarrow\; \begin{cases} \mathbf{J}\mathbf{u} + \mathbf{J}\mathbf{R}\mathbf{v} - \mathbf{R}\mathbf{C}\mathbf{v} = \lambda\mathbf{u} + \lambda\mathbf{R}\mathbf{v} \\ \mathbf{R}\mathbf{J}\mathbf{u} + \mathbf{R}\mathbf{J}\mathbf{R}\mathbf{v} - \mathbf{C}\mathbf{v} = \lambda\mathbf{v} \end{cases} \tag{S7}$$

We note that $\mathbf{u}$ is a vector that tends to the dominant eigenvector of $\mathbf{J}$ as $\mathbf{R} \to \mathbf{I}$. In that same limit, the vector $\mathbf{v}$ tends to a vector of zeroes. Slightly rearranging the eigenvector equation in [S7] yields two other useful expressions

$$\mathbf{G}^{-1}\mathbf{M}\mathbf{w} = \lambda\mathbf{G}^{-1}\mathbf{w} \;\Leftrightarrow\; \begin{cases} \mathbf{J}\mathbf{u} + \mathbf{J}\mathbf{R}\mathbf{v} = \lambda(\mathbf{I} - \mathbf{R}^2)^{-1}\mathbf{u} \\ \mathbf{C}\mathbf{v} = \lambda\mathbf{R}(\mathbf{I} - \mathbf{R}^2)^{-1}\mathbf{u} - \lambda\mathbf{v} \end{cases} \tag{S8}$$

In order to calculate $\Re(\lambda)$, we make use of the properties of the inner product $\langle \mathbf{x}, \mathbf{y} \rangle = \mathbf{x}^{\dagger}\mathbf{y}$. In particular, for any real-valued matrix $\mathbf{A}$, $\langle \mathbf{A}\mathbf{v}, \mathbf{v} \rangle = (\mathbf{A}\mathbf{v})^{\dagger}\mathbf{v} = \mathbf{v}^{\dagger}\mathbf{A}^{\mathrm{T}}\mathbf{v} = \langle \mathbf{v}, \mathbf{A}^{\mathrm{T}}\mathbf{v} \rangle$. In addition, $\langle \mathbf{v}, \lambda\mathbf{v} \rangle = \lambda\langle \mathbf{v}, \mathbf{v} \rangle$ and $\langle \lambda\mathbf{v}, \mathbf{v} \rangle = \bar{\lambda}\langle \mathbf{v}, \mathbf{v} \rangle$,

such that

$$\begin{aligned}\Re(\lambda) &= \frac{1}{2}(\lambda+\bar{\lambda}) \\ &= \frac{\langle \mathbf{v},\, \lambda\mathbf{v}\rangle + \langle \lambda\mathbf{v},\, \mathbf{v}\rangle}{2\langle \mathbf{v},\, \mathbf{v}\rangle} \\ &= \frac{\langle \mathbf{v},\, \mathbf{RJu}+\mathbf{RJRv}-\mathbf{Cv}\rangle + \langle \mathbf{RJu}+\mathbf{RJRv}-\mathbf{Cv},\, \mathbf{v}\rangle}{2\langle \mathbf{v},\, \mathbf{v}\rangle} \\ &= \frac{\langle \mathbf{Rv},\, \mathbf{J}^{\mathrm{S}}\mathbf{Rv}\rangle - \langle \mathbf{v},\, \mathbf{Cv}\rangle}{\langle \mathbf{v},\, \mathbf{v}\rangle} + \frac{\langle \mathbf{Rv},\, \mathbf{Ju}\rangle + \langle \mathbf{u},\, \mathbf{J}^{\mathrm{T}}\mathbf{Rv}\rangle}{2\langle \mathbf{v},\, \mathbf{v}\rangle},\end{aligned} \tag{S9}$$

where the long expression substituted for $\lambda\mathbf{v}$ in the third step of this calculation is taken from equation [S7]. Appearing in the final step of this derivation is the symmetric part of the matrix $\mathbf{J}$, defined as $\mathbf{J}^{\mathrm{S}} = \frac{1}{2}(\mathbf{J}+\mathbf{J}^{\mathrm{T}})$. A similar derivation, built on the result of equation [S8], gives rise to

$$\begin{aligned}\Re(\lambda) &= \frac{\langle \mathbf{u},\, \lambda(\mathbf{I}-\mathbf{R}^2)^{-1}\mathbf{u}\rangle + \langle \lambda(\mathbf{I}-\mathbf{R}^2)^{-1}\mathbf{u},\, \mathbf{u}\rangle}{2\langle \mathbf{u},\, (\mathbf{I}-\mathbf{R}^2)^{-1}\mathbf{u}\rangle} \\ &= \frac{\langle \mathbf{u},\, \mathbf{Ju}+\mathbf{JRv}\rangle + \langle \mathbf{Ju}+\mathbf{JRv},\, \mathbf{u}\rangle}{2\langle \mathbf{u},\, (\mathbf{I}-\mathbf{R}^2)^{-1}\mathbf{u}\rangle} \\ &= \frac{\langle \mathbf{u},\, \mathbf{J}^{\mathrm{S}}\mathbf{u}\rangle}{\langle \mathbf{u},\, (\mathbf{I}-\mathbf{R}^2)^{-1}\mathbf{u}\rangle} + \frac{\langle \mathbf{Rv},\, \mathbf{J}^{\mathrm{T}}\mathbf{u}\rangle + \langle \mathbf{u},\, \mathbf{JRv}\rangle}{2\langle \mathbf{u},\, (\mathbf{I}-\mathbf{R}^2)^{-1}\mathbf{u}\rangle}\end{aligned} \tag{S10}$$

We can now form a linear combination of equations [S9] and [S10], and recognize that $\langle \mathbf{v},\, \mathbf{v}\rangle + \langle \mathbf{u},\, (\mathbf{I}-\mathbf{R}^2)^{-1}\mathbf{u}\rangle = \langle \mathbf{w},\, \mathbf{G}^{-1}\mathbf{w}\rangle$, yielding a result that only depends on the symmetric part of $\mathbf{J}$:

$$\Re(\lambda) = \frac{\langle \mathbf{u}+\mathbf{Rv},\, \mathbf{J}^{\mathrm{S}}(\mathbf{u}+\mathbf{Rv})\rangle - \langle \mathbf{v},\, \mathbf{Cv}\rangle}{\langle \mathbf{w},\, \mathbf{G}^{-1}\mathbf{w}\rangle} \tag{S11}$$

Given that the matrices $\mathbf{J}^{\mathrm{S}}$ and $\mathbf{C}$ are both Hermitian (i.e., $\mathbf{J}^{\mathrm{S}} = (\mathbf{J}^{\mathrm{S}})^{\dagger}$ and $\mathbf{C} = \mathbf{C}^{\dagger}$), we next apply the following theorem from linear algebra to calculate an upper bound on $\Re(\lambda)$.

Theorem 1 (Rayleigh quotient theorem) *For any $n \times n$ Hermitian matrix $\mathbf{H}$, the Rayleigh quotient $Q(\mathbf{H},\mathbf{z}) = \langle \mathbf{Hz},\, \mathbf{z}\rangle / \langle \mathbf{z},\, \mathbf{z}\rangle$ cannot be larger than the largest eigenvalue of $\mathbf{H}$, $\Lambda_{\max}(\mathbf{H})$. Moreover, $Q(\mathbf{H},\mathbf{z}) = \Lambda_{\max}(\mathbf{H})$ if and only if $\mathbf{z}$ is equal to the eigenvector associated with the largest eigenvalue. In the same way, $Q(\mathbf{H},\mathbf{z})$ attains its minimum value when $\mathbf{z}$ is an eigenvector of $\mathbf{H}$ associated with the smallest eigenvalue $\Lambda_{\min}(\mathbf{H})$. Consequently, for any vector $\mathbf{z} \in \mathbb{C}^n$*

$$\Lambda_{\min}(\mathbf{H}) \leqslant Q(\mathbf{H},\mathbf{z}) \leqslant \Lambda_{\max}(\mathbf{H}) \tag{S12}$$

The proof of this result builds on the fact that the eigenvectors of a Hermitian matrix form an orthonormal basis of $\mathbb{C}^n$ and that the associated eigenvalues are real, so that they can be ordered.

The application of the Rayleigh quotient theorem to equation [S11] yields

$$\begin{aligned}\Re(\lambda) &= \frac{\langle \mathbf{u}+\mathbf{Rv},\, \mathbf{u}+\mathbf{Rv}\rangle Q(\mathbf{J}^{\mathrm{S}},\mathbf{u}+\mathbf{Rv}) - \langle \mathbf{v},\, \mathbf{v}\rangle Q(\mathbf{C},\mathbf{v})}{\langle \mathbf{w},\, \mathbf{G}^{-1}\mathbf{w}\rangle} \\ &\leqslant \frac{\langle \mathbf{u}+\mathbf{Rv},\, \mathbf{u}+\mathbf{Rv}\rangle \Lambda_{\max}(\mathbf{J}^{\mathrm{S}}) - \langle \mathbf{v},\, \mathbf{v}\rangle Q(\mathbf{C},\mathbf{v})}{\langle \mathbf{w},\, \mathbf{G}^{-1}\mathbf{w}\rangle} \\ &= \frac{\langle \mathbf{w},\, \mathbf{w}\rangle}{\langle \mathbf{w},\, \mathbf{G}^{-1}\mathbf{w}\rangle}\left(\left(1-\frac{\langle \mathbf{v},\, \mathbf{v}\rangle}{\langle \mathbf{w},\, \mathbf{w}\rangle}\right)\Lambda_{\max}(\mathbf{J}^{\mathrm{S}}) - \frac{\langle \mathbf{v},\, \mathbf{v}\rangle}{\langle \mathbf{w},\, \mathbf{w}\rangle}\, Q(\mathbf{C},\mathbf{v})\right)\end{aligned} \tag{S13}$$

which still depends on the relative magnitude of the two components $\mathbf{u}$ and $\mathbf{v}$ of the eigenvector $\mathbf{w}$. However, we can already infer that the sign of $\Re(\lambda)$ is determined by the sign of the weighted mean of the dominant eigenvalue of $\mathbf{J}^{\mathrm{S}}$ and the eigenvalues of $\mathbf{C}$, which are all negative. Accordingly, there is a range of values of $\Lambda_{\max}(\mathbf{J}^{\mathrm{S}})$ for which an unstable equilibrium can be stabilized, but equilibria for which $\Lambda_{\max}(\mathbf{J}^{\mathrm{S}}) < 0$ cannot become destabilized.

In order to obtain a result that explicitly depends on the intersexual correlations, we use the fact that $\mathbf{u}$ and $\mathbf{v}$ are related to each other by the second equation on the right-hand side of [S8]. As a consequence,

$$\begin{aligned}\frac{\langle \mathbf{v},\, \mathbf{v}\rangle}{\langle \mathbf{w},\, \mathbf{w}\rangle} &= \frac{\langle \mathbf{v},\, \mathbf{v}\rangle}{\langle \mathbf{v},\, \mathbf{v}\rangle + \langle \mathbf{u}+\mathbf{Rv},\, \mathbf{u}+\mathbf{Rv}\rangle} \\ &= \frac{1}{1+\frac{\langle (\mathbf{P}_\lambda+\mathbf{R})\mathbf{v},\, (\mathbf{P}_\lambda+\mathbf{R})\mathbf{v}\rangle}{\langle \mathbf{v},\, \mathbf{v}\rangle}} \\ &= \frac{1}{1+Q((\mathbf{P}_\lambda^{\dagger}+\mathbf{R})(\mathbf{P}_\lambda+\mathbf{R}),\mathbf{v})}\end{aligned} \tag{S14}$$

where $\mathbf{P}_\lambda = (\lambda\mathbf{R})^{-1}(\mathbf{C}+\lambda\mathbf{I})(\mathbf{I}-\mathbf{R}^2)$ is a complex-valued, 3×3 diagonal matrix that maps $\mathbf{v}$ to $\mathbf{u}$. Substituting this result in equation [S13] and bounding the remaining Rayleigh quotients leads to the conclusion that

$$\Re(\lambda) \leqslant \kappa \left(\Lambda_{\max}(\mathbf{J}^{\mathrm{S}}) - \left(\frac{r_{\min}|\lambda|}{|(1-r_{\min}^2)c_{\min}+\lambda|} \right)^2 c_{\min} \right) \tag{S15}$$

where $c_{\min} = \min(c_{x\sigma}, c_{z\sigma}, c_{y\varphi})$ and $r_{\min} = \min(r_x, r_z, r_y)$. Contained in the prefactor κ are several factors that are strictly positive and that, therefore, do not affect the sign of $\Re(\lambda)$, including a term that is bounded by the eigenvalues of the genetic variance-covariance matrix.

Varying one of the model's parameters in such a way that $\Re(\lambda)$ changes sign, causes a bifurcation event to occur, i.e., a qualitative change in the dynamical behavior of the model. Two different types of bifurcations can happen when $\Re(\lambda) = 0$, depending on whether the imaginary part of λ is zero at the bifurcation point or not. The first case, i.e., $\lambda = 0$, is accompanied by a change in the location (and, sometimes, the number) of equilibria, and requires that $\mathbf{M}$ is singular at the bifurcation point. Given that both $\mathbf{C}$ and $\mathbf{R}$ are positive definite, equation [S4] implies that $\mathbf{M}$ can only be singular if $\mathbf{J}$ is singular. This condition does not depend on the genetic variance-covariance matrix, so the corresponding bifurcations are independent of the intersexual genetic correlations. The reverse implication is that

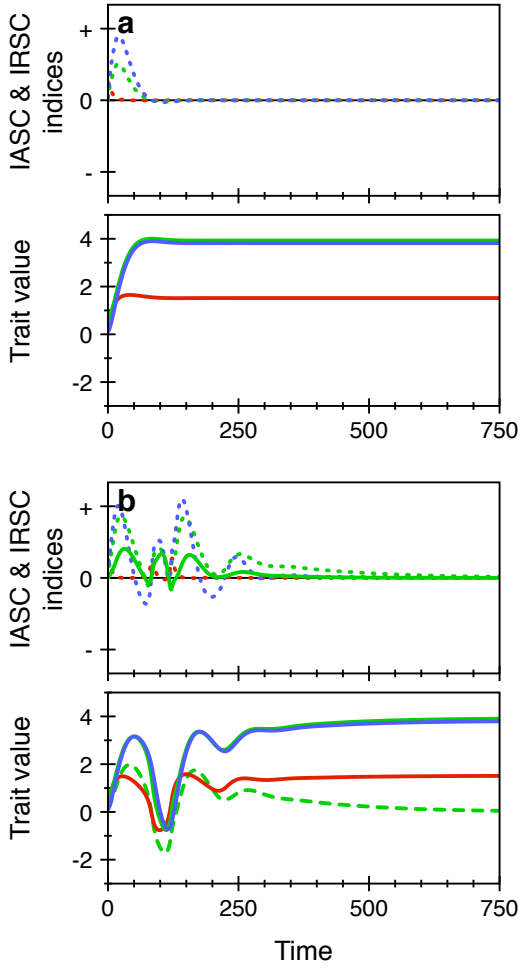

Figure S1. Dynamic of IASC and IRSC during the evolution of offense and defense traits
Similar to figure 3, each panel shows a simulation of evolving mean trait values with a corresponding timeplot of trait-specific indices of sexually antagonistic selection (dashed lines: IRSC index; solid lines: IASC index; see *Materials and Methods*). Mating is modeled as a contest between offense and defense traits. (a) Evolution in the absence of between-sex pleiotropy ($r_x = r_y = r_z = 0$). Female threshold (green) and male persistence (blue) coevolve in an escalating arms race until eventually opposed by viability selection. In (b), the approach to the equilibrium is perturbed by IASC, which can be seen to build up during phases of rapid intersexual coevolution ($r_x = 0.9$; $r_y = r_z = 0$). Pleiotropic gene expression in males constrains the evolution of the female mating threshold, inducing females to reduce their mating rate by an alternative mechanism: lowering sensitivity (red) to the mating stimulus. When females become insensitive, threshold and persistence fall back towards lower levels, initially aided by the resolution of IASC (the IASC index is negative for a brief period). Viability selection then pushes female sensitivity up again, initiating a second arms race towards positive values of threshold and persistence. This time, a slightly lower level of IASC is built up, allowing the population to converge on the equilibrium. Parameters are: $a = 5.0$, $b = 0.5$, $\theta_{x\varphi} = \theta_{x\sigma} = 0$, $\theta_{y\sigma} = \theta_{y\varphi} = 0.05$, $\theta_{z\varphi} = 0.95$, $\theta_\psi = 0.25$, $c_{x\varphi} = 0.1$, $c_{x\sigma} = c_{y\sigma} = c_{y\varphi} = c_{z\varphi} = 0.05$.

qualitative effects of intralocus conflict on the stability of intersexual selection equilibria, must involve bifurcations of the second type, known as Poincaré-Andronov-Hopf (or, Hopf) bifurcations. A Hopf bifurcation is a local bifurcation at which a pair of two complex conjugate eigenvalues crosses the imaginary axis (i.e., $\Re(\lambda)$ and $\Re(\bar{\lambda})$ change sign while $\Im(\lambda) = -\Im(\bar{\lambda}) \neq 0$). These events are associated with the birth of a limit cycle that branches from the equilibrium point.

Taking $r_{\min}$ as the bifurcation parameter of interest, we now return to inequality [S15] and ask if a Hopf bifurcation can occur when the impact of IASC increases. For equilibria that go through a Hopf bifurcation, $|\lambda| \neq 0$, which implies that the right-hand side of inequality [S15] is a strictly decreasing function of $r_{\min}^2$ in a neighborhood of the bifurcation point. Therefore, the first conclusion we can draw is that IASC has in general a stabilizing effect on the evolutionary dynamics of IRSC in the vicinity of equilibria. Furthermore, a qualitative change in the stability of an equilibrium can occur when an evolutionary fixed point is unstable under the sole action of IRSC (i.e., when $r_{\min}^2 = 0$), but when stabilizing natural selection on the homologous characters is sufficiently strong to overcome destabilizing sexual selection. In particular, if $\Re(\lambda) > 0$ at $r_{\min} = 0$, such that $\Lambda_{\max}(\mathbf{J}^{\mathrm{S}}) > 0$, and if $c_{\min} > \Lambda_{\max}(\mathbf{J}^{\mathrm{S}})$, then there is a critical value $r_{\min}^*$ such that the equilibrium is guaranteed to be stable for all $r_{\min}^* < r_{\min} \leqslant 1$.

Supplementary figures

Reversal of arms races. Here, we analyze the evolutionary trajectories of populations approaching equilibrium in order to clarify how IASC resolution reverses the direction of arms races when mating compatibility is determined by complementarity of mating traits. Simulation data are represented in two different ways in the following figures, one emphasizing the coevolutionary chase between the sexes (left column in figures S2 – S3), the other highlighting the build-up and resolution of IASC (right column in figure S2 – S3). Figure S2 shows results for the simplified model also analyzed in the main text (figure 4), for three different values of the additive genetic correlation r_x. At the lowest value of r_x (a,b; cf. figure 4a), the population can be seen to approach the green equilibrium, building up unresolved IASC on its way. The resolution of the conflict causes a temporary de-escalation of the arms race (figure S2a), due to its pleiotropic effect on $x_{♀}$. However, the population never crosses the $x_{♀} = y_{♂}$ line (dashed diagonal in a), implying that the direction of IRSC does not change qualitatively. So, after IASC has been resolved, the population resumes the coevolutionary chase until it is halted at the green equilibrium by stabilizing natural selection.

In figure S2c,d (cf. 4b), the intersexual genetic correlation is slightly stronger than in (a,b), such that higher levels of unresolved IASC build up during the arms race. By dragging down $x_{♀}$, which was ahead of $y_{♂}$ during the first phase of evolution, genetic conflict resolution switches the relative positions of the sexes in their coevolutionary chase, causing its direction to reverse. Initially aided by the natural selection gradients, this second arms race unfolds quickly, causing again high levels of IASC to build up. However, after a short phase of de-escalation, the correlated selection response is not strong enough to reverse the arms race once more, allowing the population to reach the red equilibrium.

The arms race towards the red equilibrium is more difficult to reverse, because a small asymmetry between the natural selection optima of $x_{♀}$ and $y_{♂}$ makes it slightly more difficult for the males to closely follow the females in that direction of the coevolutionary chase. Hence, higher levels of unresolved IASC are required to switch the relative positions of the sexes, as, for example, shown in figure S2e,f. Here, the population cycles several times, but note that the amount of IASC built up in the approach of the red equilibrium progressively decreases. Eventually, the population manages to resolve the genetic conflict and attain a truce with respect to intersexual conflict. At even higher levels of r_x (cf. 4d–f), full resolution of IASC is no longer feasible without triggering a new arms race, leading to perpetual coevolution between the sexes.

The argument so far considers only a single character (the female preference) that is pleiotropically expressed in the other sex. Figure S3 illustrates what happens when another trait (i.e., the male ornament) is subject to IASC instead. In this case, the correlated selection response to IASC resolution holds back the males in their pursuit of the females, enlarging rather than reversing the difference between $x_{♀}$ and $y_{♂}$. As a result, IASC resolution for male mating traits tends to preserve the direction of intersexual selection. When acting simultaneously, IASC resolution for male and female mating traits have opposite effects on the stability of intersexual antagonistic coevolution (figure S4). Arms race reversals, therefore, require stronger cross-sexual pleiotropic constraints on female mating traits (which are leading the coevolutionary chase) than on male traits (which are following behind). The scope for pleiotropy may frequently be asymmetric in this direction, as female preferences often rely on behavioral traits with a complex genetic architecture, whereas male ornamentation traits are usually highly sexually dimorphic already.

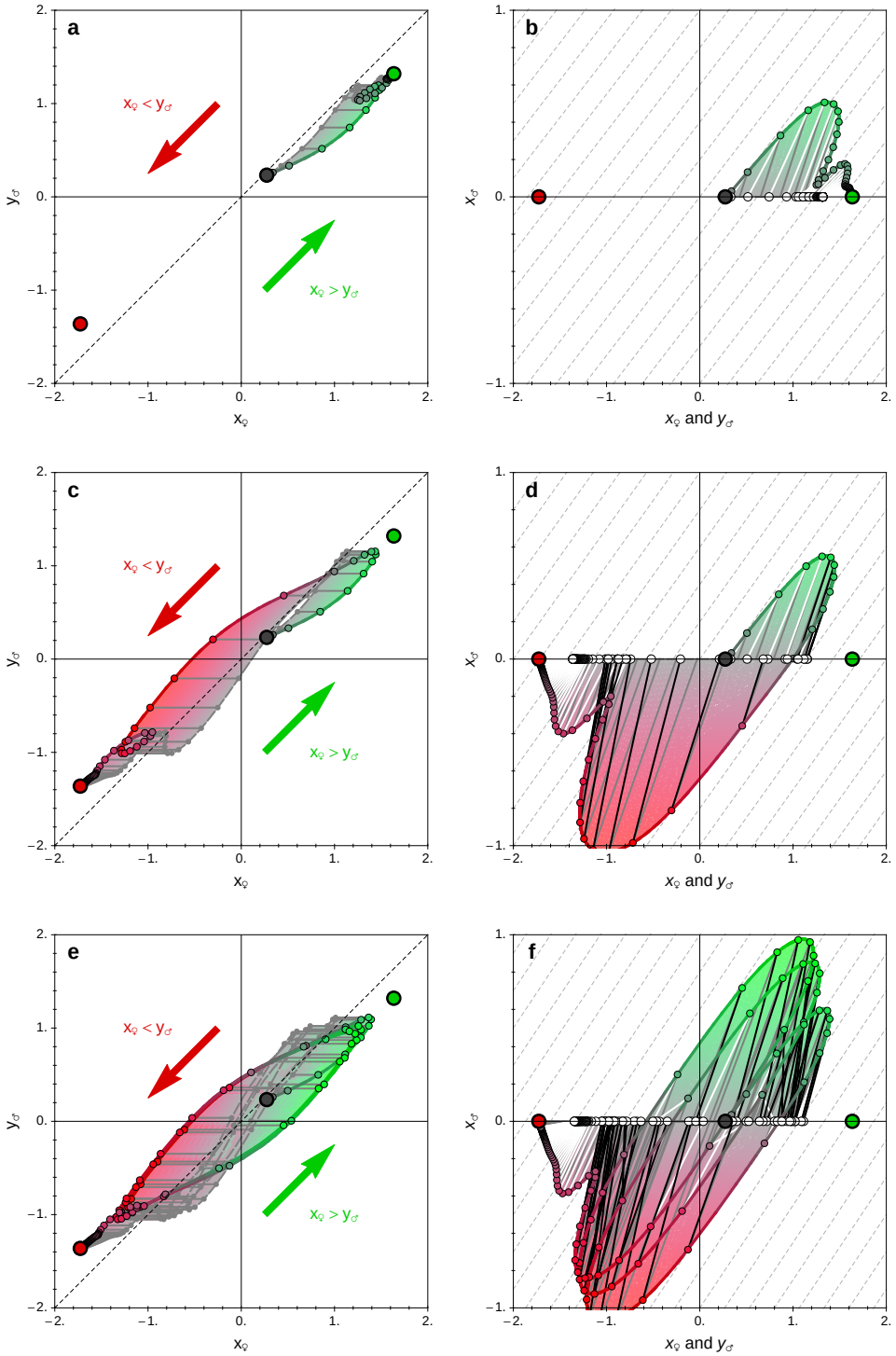

Figure S2. Pleiotropic expression of a female mating trait in males reverses the direction of arms race. Large colored dots denote the location of stable (red, green) and unstable (grey) evolutionary equilibria. Smaller open dots and colored trajectories (red/green) indicate combinations of realized trait values at regular time points during three simulations, for different levels of the intersexual genetic correlation: $r_x = 0.65$ (a and b); $r_x = 0.7$ (c and d) and $r_x = 0.75$ (e and f). Data points in the left panels show the trait values $(x_♀, y_♂)$; the corresponding right panels show the same simulations, summarized by two series of points, plotted at the coordinates $(x_♀, x_♂)$ (in red/green) and $(y_♂, 0)$ (white). Corresponding points in time of the two data series are connected by lines in (b,d,f), with different colors to indicate whether conflict resolution reverses the relative position of male and female mating traits (black → yes; white → no). This information is inferred from additional data contained in the plots: small grey dots in panel (a,c,e) indicate, at each point in time, the trait values that would result if IASC were to be fully resolved; grey lines (also present in (b,d,f)) trace the correlated selection response associated with such hypothetical, instantaneous IASC resolution. For completeness, dashed grey lines on the background of (b,d,f) also indicate the direction of trait evolution induced by IRSC and its correlated selection response. The red-green gradient used for trajectories, data points and the area of trait space that is traversed by conflict resolution provides a visual indication of the level of unresolved IASC. Parameters as in figure 4.

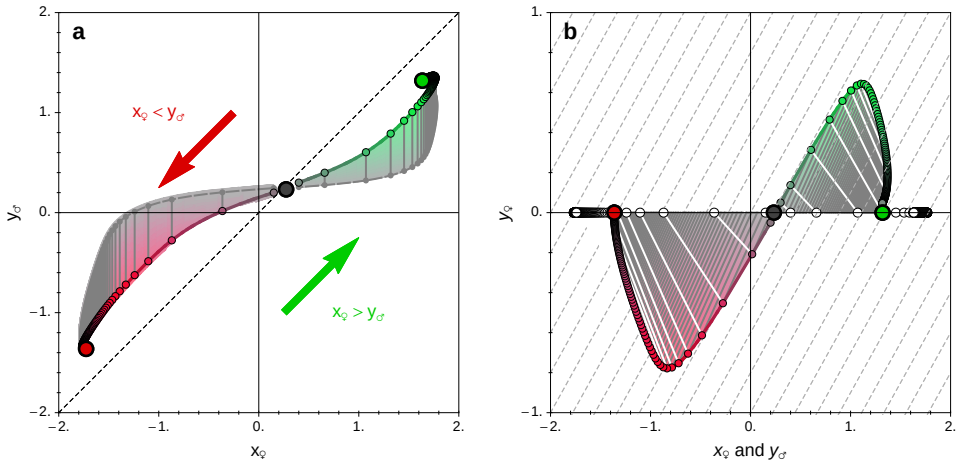

Figure S3. Pleiotropic expression of a male mating trait in females does not destabilize the approach to evolutionary equilibrium.
Conflict-resolution plots (see the legend of S2 for details) of a reduced model (female choosiness is kept fixed at $z_{♀} = 1.5$), where only the male ornament genes are pleiotropically expressed in the other sex ($r_x = r_z = 0$; $r_y = 0.9$). Each panel shows data for two simulations, started from different initial conditions on the right and on the left of the interior fixed point. Other parameters are as in figure 4.

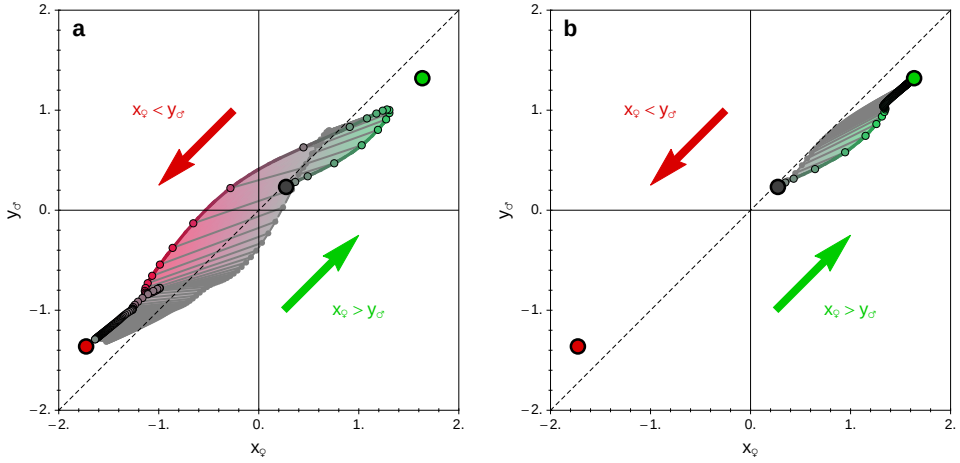

Figure S4. Combined effect of between-sex pleiotropy for male and female mating traits.
Panel (a) and (b) show two simulations of a model variant with four evolving traits ($x_{♀}$, $y_{♂}$, $x_{♂}$ and $y_{♀}$; female choosiness is kept fixed at $z_{♀} = 1.5$), i.e., both female preference and male ornamentation genes are expressed in both sexes. In (a) ($r_x = 0.9$; $r_y = 0.7$, $r_z = 0$), the destabilizing effect of IASC resolution for the preference genes (cf. figure S2) dominates, so that the coevolutionary chase leading towards the green equilibrium is reversed. In (b) ($r_x = 0.9$; $r_y = 0.8$, $r_z = 0$), IASC resolution for the male ornamentation genes has a slightly larger impact, tipping the balance in favor of preserving the direction of intersexual selection (cf. figure S3). Other parameters as in figure 4.

Global bifurcations. As a complement to the biological explanation of arms-race reversals, we used a dynamical-systems approach to illustrate how populations are drawn into a perpetual cycle of sexual conflict. The phase-diagrams in figure 4 illustrate the appearance of an alternative attractor, as a consequence of a sequence of global bifurcations. Figure S5 provides a more detailed reconstruction of the first three steps in this bifurcation sequence: the appearance of a first and second unstable limit cycle (figure S5a,b), that ultimately prevent populations from reaching equilibrium, followed by the emergence of a stable cycle that attracts the evolutionary dynamic from most initial conditions (figure S5c).

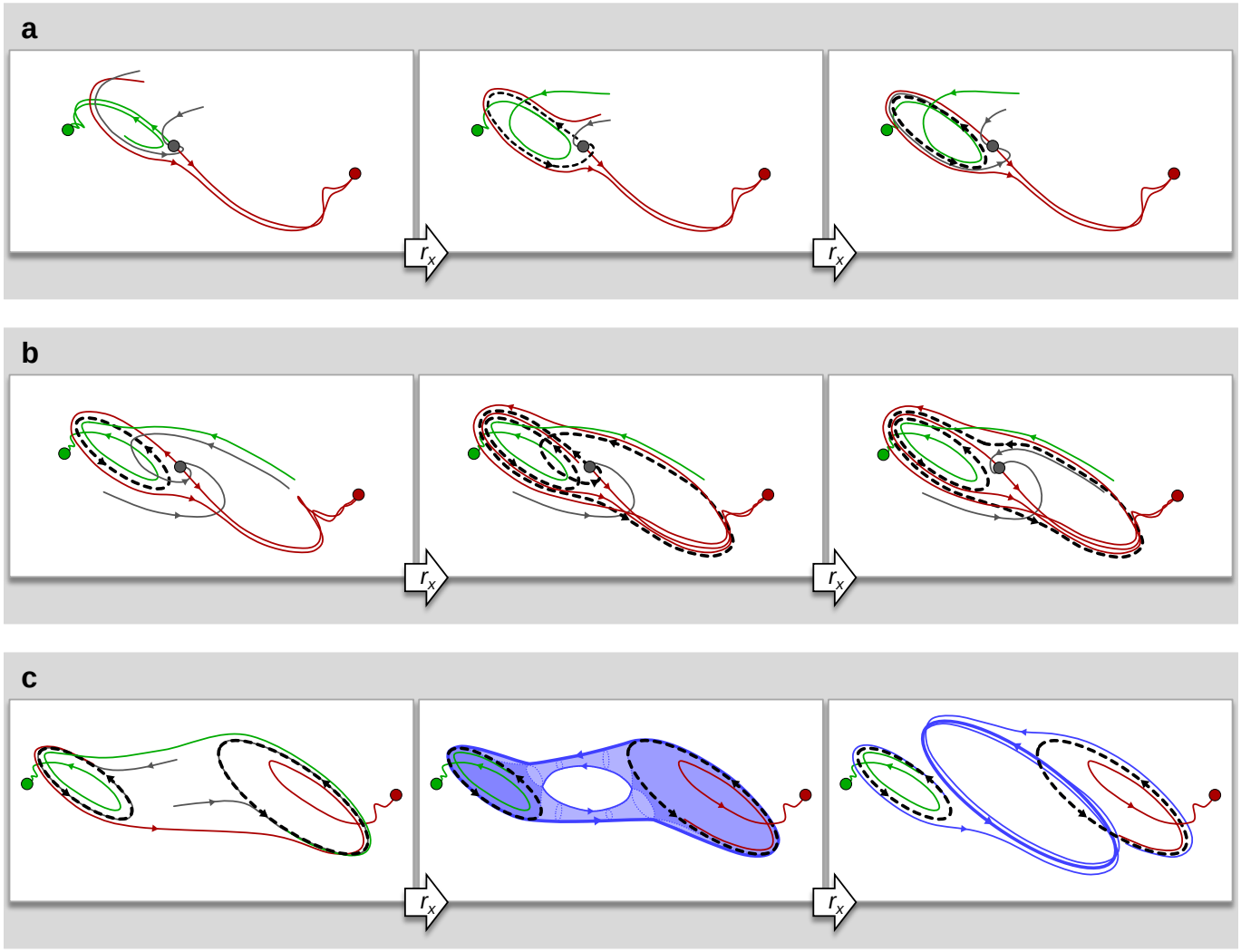

Figure S5. Global bifurcations
For each panel, schematic drawings illustrate relevant features of the phase diagram before (left), at (middle) and after (right) the point where a global bifurcation occurs. (a) *first homoclinic bifurcation*: the qualitative transition between the phasediagrams in figure 4a and b is marked by the appearance of an unstable limit cycle, which emerges from a homoclinic connection between the unstable manifold of the saddle point and the stable manifold of the same equilibrium. (b) *second homoclinic bifurcation*: at the transition between figure 4b and c, a second unstable cycle appears, due to another homoclinic connection between the stable and unstable manifolds of the interior saddle point. (c) *heteroclinic cycle-cycle connection, followed by a period-halving cascade*: the two limit cycles in figure 4c are unstable, but they attract the dynamics in one direction (i.e., they have a stable and an unstable manifold, like saddle-points). A connection between the manifolds of the two cycles gives rise to a new evolutionary attractor with the topology of a double Klein bottle. Populations evolving along the new attractor exhibit quasi-periodic behavior. The attractor quickly collapses onto a single stable limit cycle (as in figure 4d), after a cascade of period-halving bifurcations.

Coevolving choosiness. In order to simplify the model and visualize the trajectories in three dimensions, we chose to reduce the number of coevolving variables (except in the mathematical analysis and figures 1–3). This reduction was accomplished by restricting between-sex pleiotropic gene expression to a single mating character and by keeping z_{φ} fixed (corresponding to assuming an absence of genetic variation in this trait). Apart from the additional scenarios analyzed in the supplementary material (figures S3 and S4), we also confirmed the main conclusions in a model with coevolving choosiness. In this case as well, we observe the appearance of a stable evolutionary cycle that dominates the evolution of sexual conflict at higher values of the intersexual additive genetic correlation r_x (figure S6).

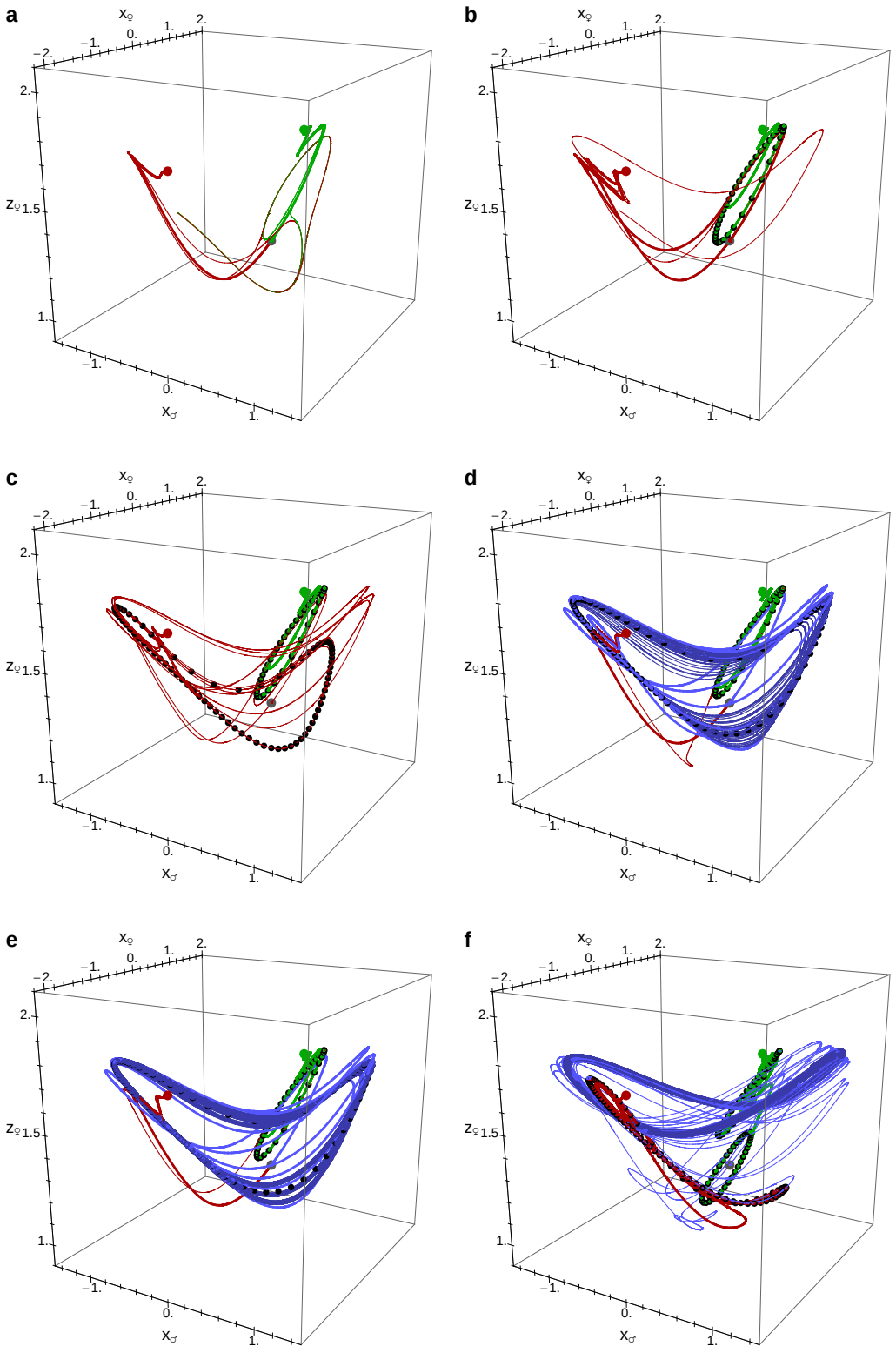

Figure S6. Destabilization of IRSC arms races with coevolving female choosiness.
The phase diagrams (a) – (f) show 3D projections of evolutionary trajectories starting from different initial conditions at six different values of the intersexual genetic correlation r_x: (a) $r_x = 0.6$; (b) $r_x = 0.65$; (c) $r_x = 0.673$; (d) $r_x = 0.677$; (e) $r_x = 0.678$ and (f) $r_x = 0.789$. Unlike in figure 4, female choosiness is not held fixed. Hence, the model has four coevolving characters, $x_♀$, $x_♂$, $y_♂$ (information on this trait is lost in the 3D projection used for visualization) and $z_♀$. (a) The starting point of the bifurcation sequence is comparable to figure 4a: there are two stable equilibria (red and green dots) separated by a saddle point (grey). (b,c) Next, two unstable cycles emerge through homoclinic bifurcations, followed by a hetero-clinic cycle-to-cycle connection that leads to quasi-periodic behavior (d). The attractor (in dark blue) then undergoes a rapid sequence of period-halving bifurcations, and in (e), it has almost collapsed into a single limit cycle. The final phase diagram (f) shows the third unstable limit cycle (cf. figure 4e), just before it disappears through a Hopf bifurcation at the interior equilibrium point. Parameters as in figure 3 with $r_y = r_z = 0$.

Individual-based simulations. Individual-based simulations were implemented in C^{++}, closely following the assumptions of the quantitative-genetic model. The simulation program keeps track of a population of N individuals with equal proportions of males and females. Each individual carries separate sets of gene loci for x, y and z. Some of the loci are expressed in both sexes, others have sex-limited expression, so that the intersexual additive genetic correlation can be varied by modifying the proportion of sex-limited genes. We allowed for two alleles (denoted + and –) to segregate at a locus and included a low rate of mutation to introduce new genetic variation. Phenotypic trait values are calculated based on the assumption of additive gene action, i.e., each + allele increases the trait value by an amount $\delta/2$, whereas a – allele decreases the trait value by $\delta/2$.

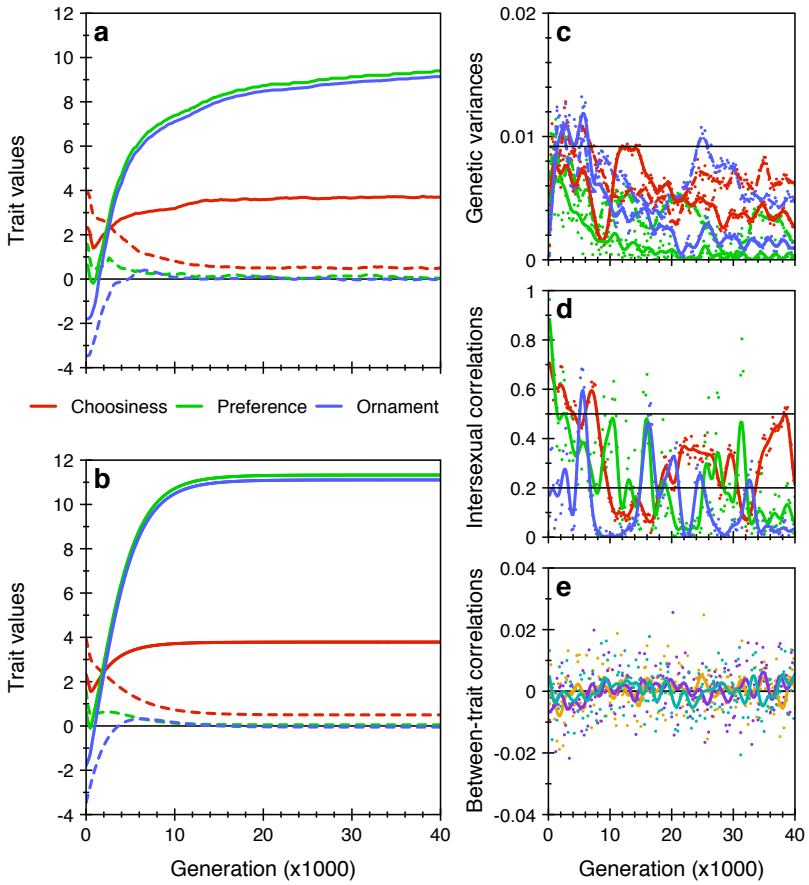

Figure S7. Comparison between individual-based simulation and quantitative-genetic predictions
For the same parameters as in figure 2a, the evolution of the mating traits (solid lines) and correlated characters (dashed lines) was modeled using a stochastic individual-based simulation. The trajectory of the mean trait values in a simulated population of $N = 10000$ individuals (a) matches in detail with the corresponding prediction from the quantitative genetic model [S19] (b), except for minor differences in the rate of convergence to the equilibrium and the equilibrium trait values. These qualitative differences relate to discrepancies between the observed (colored lines) and predicted (black lines) genetic variances (c) and intersexual genetic correlations (d), which are a consequence of the genetic architecture of the traits in the individual-based simulation (see discussion in text). Each phenotypic character was determined by $L = 600$ haploid, bi-allelic loci. Some of these were expressed in both sexes and therefore affected a mating character and a correlated character in the other sex: the phenotypic characters x_{φ} and x_{σ} were assumed to share a common genetic basis of $K_x = 300$ loci (so that 300 loci exhibited sex-specific expression; $r_x = 300 / 600 = 0.5$), y_{σ} and y_{φ} shared $K_y = 120$ loci (implying that each was also affected by 480 sex-specific loci; $r_y = 120 / 600 = 0.2$) and z_{φ} and z_{σ} shared again $K_z = 300$ loci ($r_z = 300 / 600 = 0.5$). Mutations occurred at a rate of 0.001 per genome per generation (corresponding to a rate of $\mu = 3.47 \times 10^{-7}$ per gene copy). The phenotypic effect size of mutations was set to $\delta = 1/15$, allowing all trait values to range from -20 to 20. Panel (e) shows the values of the average additive genetic correlations between traits (orange: choosiness × preference; purple: choosiness × ornament; blue-green: preference × ornament). Between-trait correlations are ignored in the quantitative genetic model, but may evolve in the individual-based simulation due to non-random mating and genetic drift, potentially affecting the evolutionary trajectory. Lines in (c-e) represent smoothed data (low-pass filter; data-reduction factor 4); raw data are indicated by dots.

Each generation in the simulation program proceeds in three steps. First, the phenotypes of individuals are determined from their genotype, depending on whether the individual is male or female. Second, the viability of each individual is calculated taking into account stabilizing viability selection on the mating traits and the homologous characters. The last step in the life-cycle is the production of offspring. Here, in contrast to the quantitative genetic model, we did not evaluate reproductive success based on the population average trait values. Rather, the mating process was implemented in a more mechanistic fashion, allowing us to obtain a stronger validation of the quantitative

genetic model: for every offspring, the simulation algorithm first randomly picks a female from the population of surviving females. This female is then assumed to encounter $n = 50$ different males sampled randomly from the surviving males. The mating rate of the focal female with each of the males (denoted by ψ_i for the i-th male) is evaluated. Next, a single mating partner is picked for the focal female from the sample of n males. This sampling step is implemented as a weighted lottery with weights given by male relative reproductive success $\exp(b\,\psi_i)$. The reproductive success of the female determines the probability that she will produce an offspring from the current mating attempt. Female reproductive success is calculated as $\exp(-a \sum_{1 \leqslant i \leqslant n} (\psi_i - \theta_\psi)^2/(2n))$, i.e., assuming multiplicative costs of interactions with all the n males encountered by the female. The procedure is repeated until $N/2$ male and $N/2$ female offspring are produced. All surviving males and all surviving females are available to participate in each mating attempt, irrespective of how many mating attempts they have participated in already. After all offspring have been created, the parental generation is removed from the memory and replaced by their offspring. Inheritance was implemented assuming either haploid or diploid genetics and free recombination between loci.

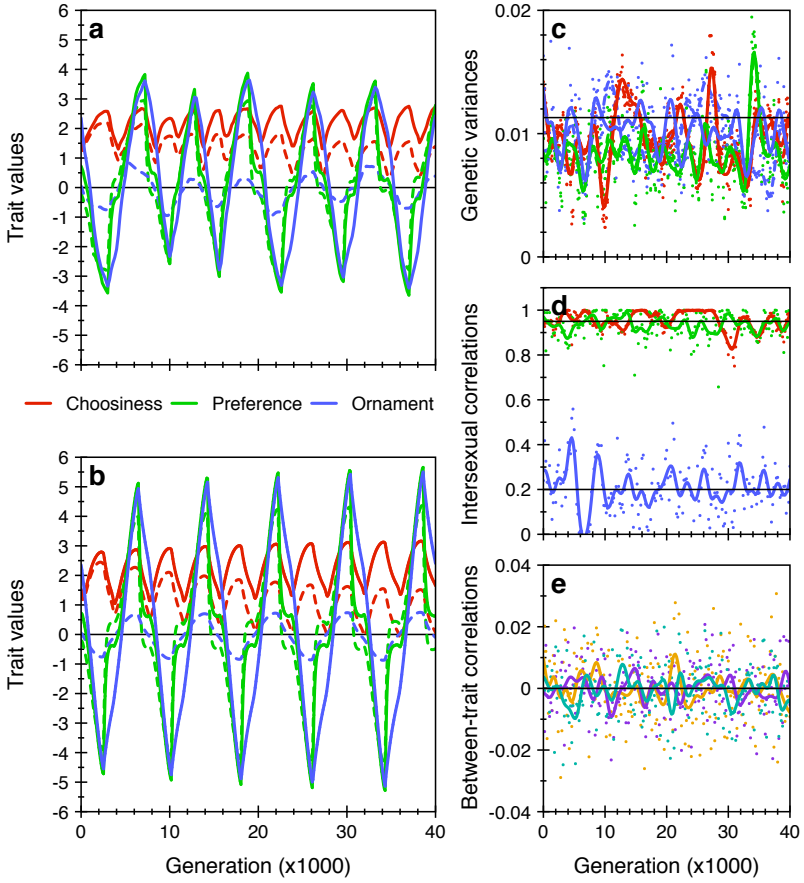

Figure S8. Occurrence of oscillations in an individual-based simulation
The correspondence between individual-based simulation results (a) and the quantitative-genetic model (b) extends to the parameter regime where oscillations occur (parameters are as in figure 2b). In this simulation, the evolving trait values remain far from the edges of the feasible phenotype range (from -20 to +20) and selection is weak, such that the between-trait correlations (e) remain negligible and the observed genetic variances (c) and intersexual correlations (d) match well with their expected values (black lines) based on equation [S19]. Population size and genetic parameters were as in figure S7 (see the legend of that figure for further details), except that K_x and K_z were increased to 570 ($r_x = r_z = 570 \,/\, 600 = 0.95$). This also had an effect on the per-locus mutation rate, which increased to $\mu = 4.27 \times 10^{-7}$, still corresponding to a genomic mutation rate of 0.001 per generation.

To ensure correspondence between the generation time in the individual-based simulations and the time units of the quantitative-genetic model, we scaled the time variable of the breeder's equation [S1] by a factor 2 to take into account that each of the phenotypic characters is exposed to selection in only half of the individuals (i.e., either in males or in females). In addition, estimates for the elements of the **G**-matrix were derived from the parameters of the individual-based simulation, using approximations from the neutral theory of molecular evolution. In particular, under the assumptions of the infinite-alleles model [4], the probability F that a single locus is homozygous at mutation-drift equilibrium in a diploid population of size N is given by $F = 1/(1 + 4\mu N)$, where μ is the mutation rate. Given that the genetic variance at the locus is half of the heterozygosity, $1 - F$, we can now estimate V_L the additive genetic variance of a neutral phenotypic character that is encoded by L diploid loci:

$$V_L = 2L \times \frac{1}{2}\left(1 - \frac{1}{1 + 4\mu N}\right) \times \delta^2 = L\delta^2 \frac{4\mu N}{1 + 4\mu N}, \tag{S16}$$

where δ is the phenotypic effect of a mutation. Similarly, the additive genetic covariance C_K between two neutral phenotypic characters that share a common genetic basis of K loci is given by

$$C_K = K\delta^2 \frac{4\mu N}{1+4\mu N}. \tag{S17}$$

The amount of additive genetic (co)variation that is present for phenotypic characters that are subject to selection is expected to converge to the neutral expectation (equations [S16] and [S17]) in the limit of weak selection. Hence, if selection is weak, we expect that the dynamic of the individual-based simulation is captured approximately by the following breeder's equation:

$$\frac{d\mathbf{u}}{dt} = \frac{1}{2}\begin{pmatrix} V_L & 0 & 0 & C_{K_x} & 0 & 0 \\ 0 & V_L & 0 & 0 & C_{K_z} & 0 \\ 0 & 0 & V_L & 0 & 0 & C_{K_y} \\ C_{K_x} & 0 & 0 & V_L & 0 & 0 \\ 0 & C_{K_z} & 0 & 0 & V_L & 0 \\ 0 & 0 & C_{K_y} & 0 & 0 & V_L \end{pmatrix} \boldsymbol{\beta}(\mathbf{u}) = \frac{1}{2} L\delta^2 \frac{4\mu N}{1+4\mu N} \begin{pmatrix} 1 & 0 & 0 & K_x/L & 0 & 0 \\ 0 & 1 & 0 & 0 & K_z/L & 0 \\ 0 & 0 & 1 & 0 & 0 & K_y/L \\ K_x/L & 0 & 0 & 1 & 0 & 0 \\ 0 & K_z/L & 0 & 0 & 1 & 0 \\ 0 & 0 & K_y/L & 0 & 0 & 1 \end{pmatrix} \boldsymbol{\beta}(\mathbf{u}) \tag{S18}$$

Here, we have assumed (as in the individual-based simulations) that the number of loci coding for each phenotypic character (L) and the phenotypic effect of a mutation (δ) are identical for all characters. The number of loci that are shared between male and female characters however, are allowed to differ between traits, so that K_x, K_y and K_z can be varied to control the degree of between-sex pleiotropy for each character independently. As mentioned above, the factor 1/2 in front of the **G**-matrix appears because each phenotypic character is subject to selection in only one sex.

Equation [S18] applies to a diploid population. The analogous equation for a haploid population is given by

$$\frac{d\mathbf{u}}{dt} = \frac{1}{4} L\delta^2 \frac{2\mu N}{1+2\mu N} \begin{pmatrix} 1 & 0 & 0 & K_x/L & 0 & 0 \\ 0 & 1 & 0 & 0 & K_z/L & 0 \\ 0 & 0 & 1 & 0 & 0 & K_y/L \\ K_x/L & 0 & 0 & 1 & 0 & 0 \\ 0 & K_z/L & 0 & 0 & 1 & 0 \\ 0 & 0 & K_y/L & 0 & 0 & 1 \end{pmatrix} \boldsymbol{\beta}(\mathbf{u}) \tag{S19}$$

Accordingly, for the same value of L and all other parameters, a haploid population evolves up to four times more slowly than a diploid population. The difference is due to two factors: first, relative to a diploid, a haploid individual carries only half the amount of gene copies, and therefore accumulates mutations at half the rate of a diploid individual; second, mutations are more rapidly lost from a haploid population, due to the smaller effective population size of its gene pool. As a result, the amount of genetic variation maintained at mutation-drift equilibrium in a haploid population is up to two times lower than in a diploid population.

Figures S7 and S8 compare the quantitative-genetic predictions based on equation [S19] with individual-based simulation results. The trajectories predicted by the two methods are, overall, in good agreement, both for a simulation that shows an arms race towards a stable equilibrium (figure S7a,b) and for one that exhibits oscillations (figure S8a,b). As expected, the additive genetic variances (panel S7c and S8c) are slightly lower in the individual-based simulation than predicted by equation [S16], since part of the variation is eroded by selection. However, given the observed time-scale correspondence between the two modeling methods, this discrepancy appears to have relatively minor consequences for the predicted rate of adaptive evolution.

Since we do not allow the allelic effect sizes or the number of loci to evolve, the phenotypic trait values in the individual-based simulations are restricted to a finite range (between $-L\delta/2$ and $+L\delta/2$ for haploid genetics). This constraint has three consequences that are ignored in the quantitative-genetic model. First, the maximal genetic variance decreases with the absolute mean trait value in the individual-based simulation, an effect that can clearly be observed in figure S7c after generation 10000. Second, also the intersexual correlations are constrained by the finite genetic architecture of the traits when the mean trait values evolve towards the end points of the feasible phenotype range. This effect is only weak in figure S8d, but appreciable in figure S7d where systematic deviations of the intersexual correlations from their expected values are observed after generation 10000. Third, mutation can only act in one direction at the extreme ends of the feasible phenotype range and generally has a tendency to bias evolution towards trait value 0. Consistent with these three effects, the individual-based simulation shows a retarded approach to equilibrium at lower escalated trait values (figure S7a).

Mutation bias may also partially explain why the amplitude of the oscillations in the individual-based simulations is less than predicted by the quantitative-genetic model (figure S8a,b). However, additional simulations show that the discrepancy in amplitude also depends on the population size (figure S9) and other factors that influence the amount of standing genetic variation (mutation rate, number of loci and allelic effect size). Therefore, we hypothesize that the presence of genetic variation, which is not taken into account in the derivation of the selection gradients, causes the arms race to reverse prematurely, reducing the amplitude of the evolutionary oscillations. Data recorded from simulations across a range of population sizes are consistent with this hypothesis (figures S9 and S10). The same simulations also validate the quantitative genetic model [S18] for diploid populations.

Surprisingly, the predicted dynamics of the quantitative-genetic model is mirrored most accurately in relatively small populations, even though the impact of genetic drift on evolution is generally inversely related to population size. The pattern suggested by figure S9 is confirmed by a more careful quantification of the period and amplitude of the evolutionary oscillations observed in the individual-based simulations (figure S10). Close correspondence between the two modelling methods is found for populations smaller than 20000 individuals, whereas substantial deviations

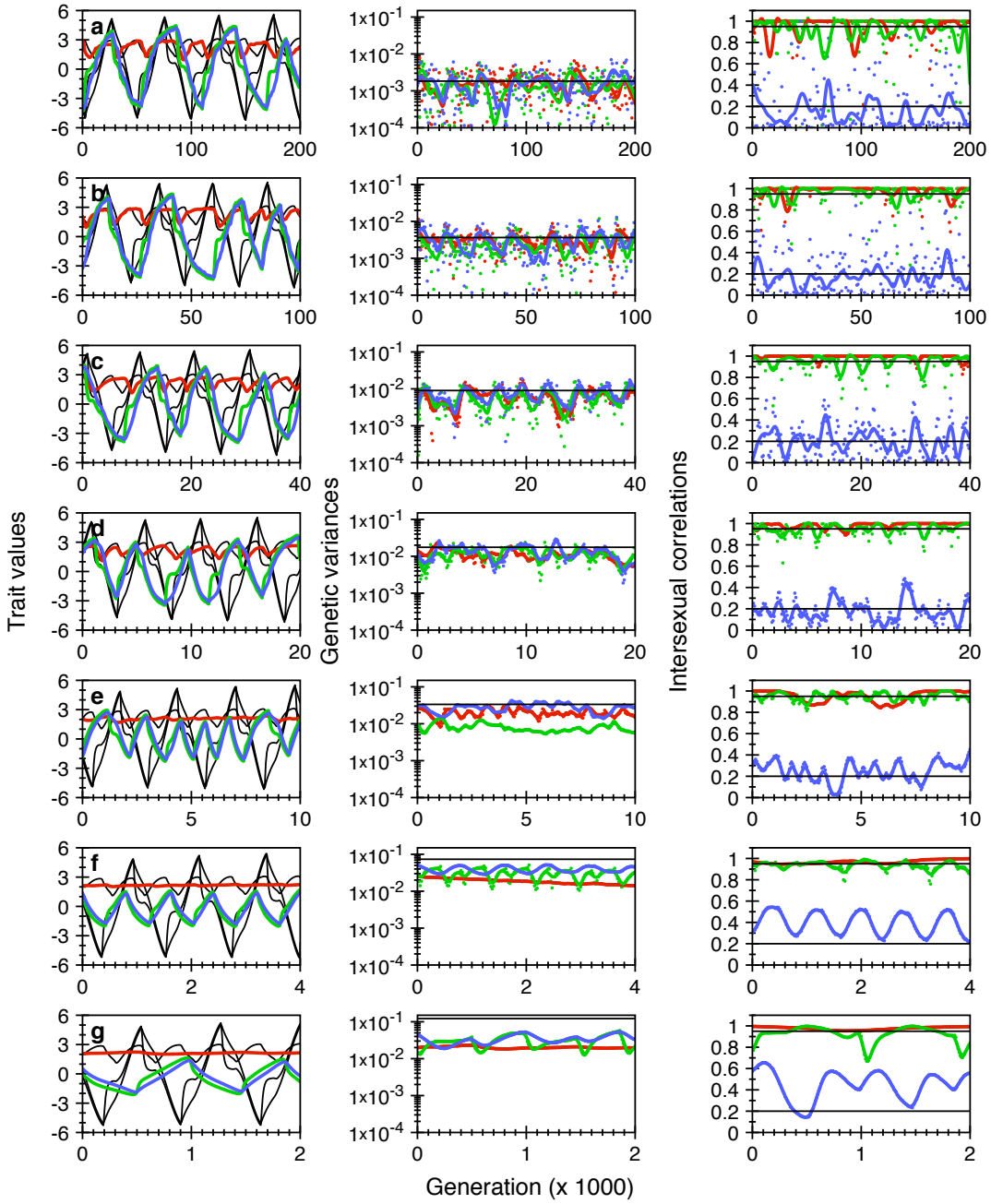

Figure S9. Individual-based simulations of diploid populations across a range of population sizes
Also for diploid populations, individual-based simulations show evolutionary oscillations, in agreement with the predictions of the quantitative-genetic model (parameters are as in figure 2b). Across a range of population sizes (row (a): $N = 1000$; (b): $N = 2000$; (c): $N = 5000$; (d): $N = 10000$; (e): $N = 20000$; (f): $N = 50000$; (g): $N = 100000$) the three columns show, respectively, the dynamic of average trait values for the mating characters, their additive genetic variances and the intersexual genetic correlations r_x, r_z and r_y. Throughout, individual-based simulation results are shown in color, whereas the corresponding quantitative genetic predictions are shown in black. Quantitatively, the agreement between simulation results and quantitative genetic predictions is better at the lower population sizes, despite the dynamics of the genetic variances (middle column) and the larger effect of genetic drift, which are ignored by the breeder's equation [S18]. As population size increases, the amplitude of the oscillations in the individual-based simulation decreases, presumably due to the presence of higher levels of standing genetic variation in large populations. A systematic change in the dynamics occurs at population size 20000 and above (panel e-g): here the genetic variances and intersexual correlations start to exhibit regular oscillations, and the dynamic of the average trait values slows down. Genetic parameters are: $L = 100$ diploid loci, $K_x = K_z = 95$, $K_y = 20$, $\delta = 0.06$, $\mu = 1.28 \times 10^{-6}$corresponding to a genomic mutation rate of 0.001. As before, raw data (dots) are presented along with smoothed data (lines) in the middle and right column of panels.

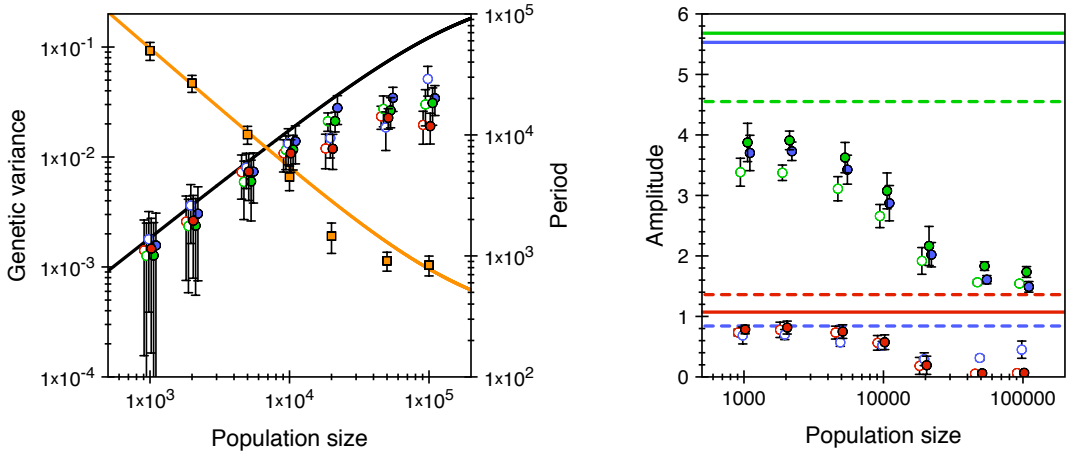

Figure S10. Period and amplitude of the oscillations in the individual-based simulation model
The simulations shown in figure S9 were extended to include 10 full evolutionary cycles, from which we estimated the average period (a; orange filled squares) and amplitude (b) of the oscillations as a function of the population size. Lines show corresponding predictions from the quantitative genetic model [S18]. Also shown in (a) are the average additive genetic variances observed in the simulations, for the mating characters (red, blue and green filled circles for choosiness, preference and ornament, respectively) and their correlated characters (corresponding open circles). The same symbols are used in (b) to indicate the amplitude of the oscillations for each trait (line styles for the predicted values follow the convention used in earlier figures). Throughout, error bars indicate the standard deviation of the estimates obtained from the individual-based simulations. Data points have been slightly displaced in the horizontal direction to improve clarity.

in amplitude and period occur in populations larger than that size. The two outcomes coincide with two distinct population-genetic regimes: if $4\mu N \ll 1$, evolution is mutation-limited, the amount of genetic variation present in the population is low and adaptation proceeds as a sequence of discrete mutation and trait-substitution events; by contrast $4\mu N > 0.1$ when $N > 20000$ (given that $\mu = 1.28 \times 10^{-6}$), implying that an appreciable level of standing genetic variation is present in the largest simulated populations.

Previous models of IRSC have shown that the presence of genetic variation can give rise to frequency-dependent selection favoring further diversification, a self-reinforcing process that can dramatically alter the outcome of evolution [3]. Since these effects have not been incorporated in the derivation of the selection gradients, the maintenance of genetic polymorphism by frequency-dependence provides a likely explanation for the observed discrepancies at high population size. To support this intuition, we ran simulations at which high levels of standing genetic variation were expected. An example is shown in figure S11. Here, $4N\mu = 25.6$, and the additive-genetic variances reach high values (figure S11c) compared to the earlier simulations. Females, in particular, exhibit extensive genetic variation in preference, supported by negative frequency-dependent selection. As a consequence, it is impossible for a single male phenotype to realize a high mating rate across the full spectrum of available female mating types (i.e., this is the 'Buridan's ass' scenario, described in earlier studies of sexual conflict [3]). Phenotypic diversification enables the females to escape male harassment, while keeping the males trapped at an intermediate compromise phenotype. Therefore, sexual conflict no longer generates directional arms races in the simulation of figure S11, and the evolutionary oscillations predicted by our model have reduced to subtle periodic fluctuation of the population mean values of preference and ornamentation (barely visible in figure S11a).

To complete the analysis, we ran individual-based simulations of the mating-contest scenario. Unlike the other simulations, which were first run for a while to allow genetic variation to build up, these simulations were started with a population of genetically identical individuals from which data were recorded immediately. This was necessary to enable the visualisation of the transient dynamics. The low initial genetic variation in the simulation caused the initial dynamic to slow down, but otherwise the match between simulation data and the quantitative-genetic model was satisfactory (figure S12): we recovered the expected qualitative contrast between sustained oscillations and convergence to a stable equilibrium at low and high intersexual correlations, respectively. However, the oscillations in the individual-based simulations were slower and had a lower amplitude. These effects appear to be due mainly to a reduction of the genetic variance for the female mating threshold.

In summary, we conclude that the individual-based simulations (figures S7-S12) alltogether confirm the robustness of our main results. In particular, the quantitative genetic model, with its assumption of a constant **G**-matrix was shown to provide an adequate description of the evolutionary dynamic in a genetically explicit individual-based model implementation, in the limit of weak selection and mutation-limited evolution (figures S7-S8). Moreover, the main findings extend qualitatively beyond this regime, up to the point where the maintenance of standing genetic variation opens up alternative possibilities (e.g., phenotypic diversification) for the evolutionary outcome of sexual conflict (figures S9-S11).

Several processes included in the individual-based simulations could have potentially undermined the predictions of the quantitative genetic model: (1) genetic variation in the direction of the selection gradient is reduced by selection, both as a result of a change of mean allele frequencies, and by generating linkage disequilibria between selected loci [5]; (2) non-random mating generates a genetic correlation between male and female mating characters, which is ignored in our main analysis; (3) each character is coded by a finite number of loci, introducing mutation bias (as a function of trait value) and other side-effects of a finite genetic architecture, and (4) genetic drift produces random gene-frequency change and linkage disequilibria that potentially interfere with adaptive evolution. Signatures of each of these effects were observable in the individual-based simulations, and in some cases, the genetic variances and covariances were found to evolve dynamically (e.g., figure S9f,g). Yet, the joint effect of the deviations from the assumed fixed **G**-matrix was relatively minor (except in figure S11, by construction). The observed robustness of the quantitative-genetic predictions results from the fact that the evolving characters were modeled as quantitative traits coded by many freely recombining loci: accordingly, the strength of selection is diluted over many loci, while linkage disequilibria are broken down effectively by recombination. Theory [6] predicts that, in this regime, indirect selection mediated by linkage disequilibria can be ignored relative to direct selection (including selection on pleiotropic characters), so that the fixed **G**-matrix assumed in the quantitative-genetic analysis provides a correct first-order approximation for the evolving genetic architecture in the individual-based simulations. A clear illustration of this point is provided by the linkage disequilibrium generated by mate choice, which is not taken into account in the quantitative-genetic analysis. Despite strong sexual selection and non-random mating, the expected positive genetic correlation between preference and ornament is hardly detectable in the simulations (figure S7e, S8e), except when high genetic variation is present, as in figure S11.

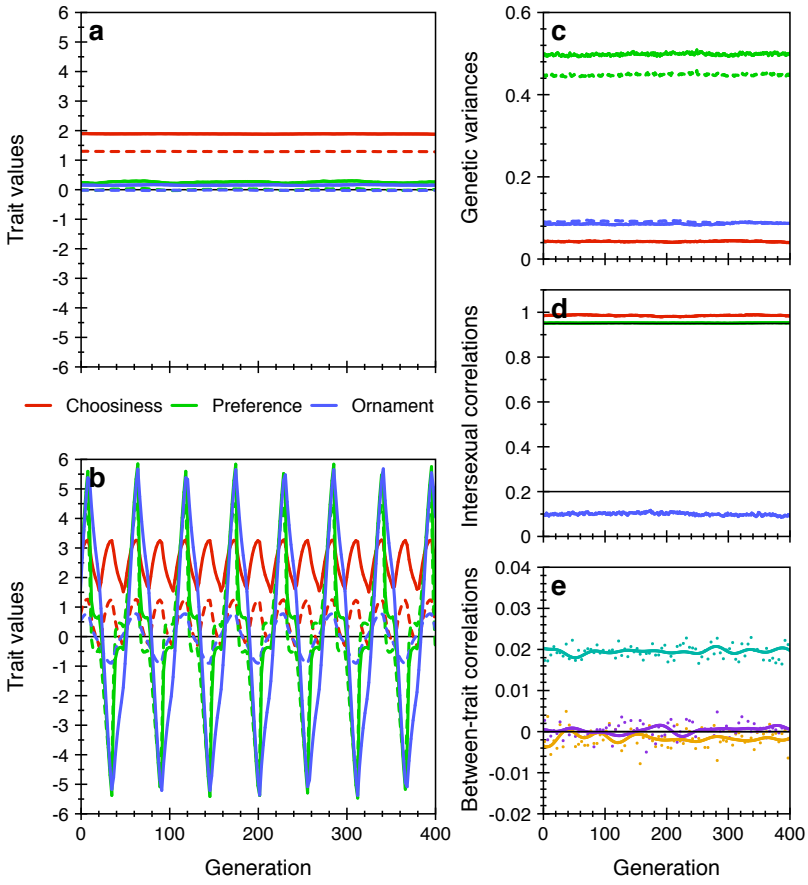

Figure S11. Diversification of mating preferences supported by frequency dependent selection
The maintenance of high levels of standing genetic variation in this simulation opens up the possibility for females to diversify, thus allowing them to permanently escape male harassment. The signatures of this so-called 'Buridan's ass' scenario [3] are apparent in (a) and (c): the additive genetic variance of the female mating preference is much higher than that of the male ornament, and directional arms races have been replaced by subtle fluctuations of the frequency distributions generated by negative frequency-dependent selection. (b) Under the weak-selection assumption of the quantitative genetic model, the variation in the population is ignored, so that the breeder's equation [S18] fails to predict the evolutionary trajectories. As before, panel (d) and (e) show the additive genetic intersexual correlations and between-trait correlations, respectively. Note that the correlation between preference and ornament is 2%, due to non-random mating. Parameters are: $N = 100000$, $L = 20$ diploid loci, $K_x = K_z = 38$, $K_y = 8$, $\delta = 0.3$, $\mu = 6.41 \times 10^{-5}$, corresponding to a genomic mutation rate of 0.01; other parameters as in figure 2b.

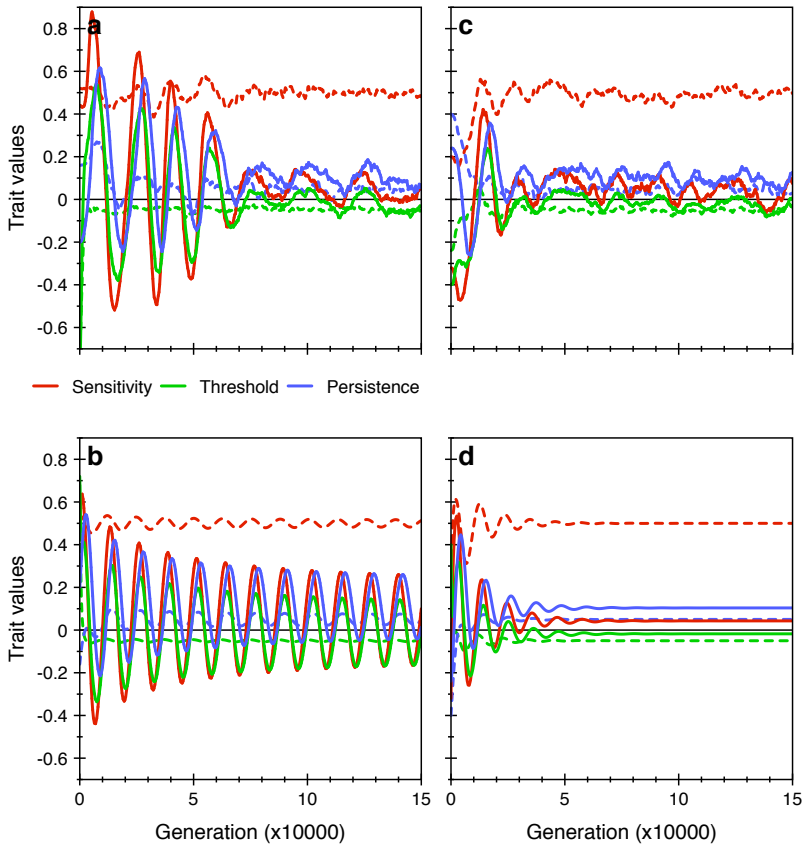

Figure S12. Individual-based simulations of the contest mating scenario
Evolutionary oscillations of male offense and female defense traits are stabilized by between-sex pleiotropic gene expression in individual-based simulations (upper panels), in agreement with the corresponding runs of the quantitative-genetic model (lower panels). (a) At low values of the intersexual genetic correlations ($r_x = r_z = 0.1$; $r_y = 0.2$), the mating traits show regular oscillations, but with a smaller amplitude and longer period than in the quantitative-genetic model (b). These quantitative differences are the result of a reduced genetic variance in the female mating threshold, which causes this trait to lag behind in the oscillations during the second half of the simulation. (c) The regular oscillations are lost at higher values of the intersexual genetic correlations ($r_x = r_z = 0.5$; $r_y = 0.2$), in line with the results of the quantitative genetic model (d). However, the individual-based simulation continues to show irregular, damped oscillations around the equilibrium point, as a result of genetic drift. Parameters: $a = 5$, $b = 0.5$, $\theta_{x_♀} = \theta_{x_♂} =$ -0.05, $\theta_{y_♀} = \theta_{y_♂} = 0.05$, $\theta_{z_♀} = \theta_{z_♂} = 0.5$, $\theta_\psi = 0.2$, $c_{x_♀} = c_{x_♂} = 0.5$, $c_{y_♀} = c_{y_♂} = c_{z_♀} = c_{z_♂} = 0.1$, $N = 25000$, $L = 500$ haploid loci, $K_x = K_z = 50$ in (a) and $K_x = K_z = 250$ in (b), $K_y = 100$, $\delta = 0.04$, $\mu = 3.57 \times 10^{-7}$ in (a) and $\mu = 4.17 \times 10^{-7}$ in (b), both corresponding to a genomic mutation rate of 0.001.

References

[1] Lande R, Arnold SJ (1983) The measurement of selection on correlated characters. *Evolution* 37:1210–1226.

[2] Rowe L, Cameron E, Day T (2005) Escalation, retreat, and female indifference as alternative outcomes of sexually antagonistic coevolution. *Am. Nat.* 165:S5–S18.

[3] Gavrilets S (2014) Is sexual conflict an engine of speciation? *Cold Spring Harb. Persp. Biol.* 6: a017723.

[4] Kimura M, Crow J (1964) The number of alleles that can be maintained in a finite population. *Genetics* 49: 725–738.

[5] Bulmer MG (1971) The effect of selection on genetic variability. *Am Nat* 105: 201–211.

[6] Kirkpatrick M, Johnson T, Barton N (2002) General models of multilocus evolution. *Genetics* 161: 1727–1750.